



UNIVERSITY OF LEEDS

This is a repository copy of *Selective recovery of lithium from spent coin cell cathode leachates using ion imprinted blended chitosan microfibers: Pilot scale studies provide insights on scalability.*

White Rose Research Online URL for this paper:

<https://eprints.whiterose.ac.uk/185340/>

Version: Accepted Version

Article:

Das, D, R, A, Kay, P orcid.org/0000-0002-9997-7860 et al. (3 more authors) (2022) Selective recovery of lithium from spent coin cell cathode leachates using ion imprinted blended chitosan microfibers: Pilot scale studies provide insights on scalability. *Journal of Hazardous Materials*, 431. 128535. ISSN 0304-3894

<https://doi.org/10.1016/j.jhazmat.2022.128535>

This manuscript version is made available under the CC-BY-NC-ND 4.0 license
<http://creativecommons.org/licenses/by-nc-nd/4.0/>.

Reuse

This article is distributed under the terms of the Creative Commons Attribution-NonCommercial-NoDerivs (CC BY-NC-ND) licence. This licence only allows you to download this work and share it with others as long as you credit the authors, but you can't change the article in any way or use it commercially. More information and the full terms of the licence here: <https://creativecommons.org/licenses/>

Takedown

If you consider content in White Rose Research Online to be in breach of UK law, please notify us by emailing eprints@whiterose.ac.uk including the URL of the record and the reason for the withdrawal request.



eprints@whiterose.ac.uk
<https://eprints.whiterose.ac.uk/>

Selective recovery of lithium from spent coin cell cathode leachates using ion imprinted blended chitosan microfibers: Pilot scale studies provide insights on scalability

Devlina Das^{a,b}, Abarajitha R^b, Paul Kay^c, V. Ramamurthy^{b,d}, Francisco M. Goycoolea^a, Nilanjana Das^e

^a School of Food Science and Nutrition, University of Leeds, LS2 9JT, United Kingdom

^b Department of Biotechnology, PSG College of Technology, Coimbatore 641004, India

^c School of Geography, University of Leeds, LS2 9JT, United Kingdom

^d Department of Biomedical Engineering, Sri Ramakrishna Engineering College, Coimbatore 641 022, India

^e Bioremediation Laboratory, School of Biosciences and Technology, Vellore Institute of Technology, Vellore 632014, India

1. Introduction

Recovery of value-added metals from spent battery cathodes is worthy to be considered in terms of value addition, cost of operation and environmental impacts. Among value-added elements, lithium is a versatile one with diverse application areas. The global demand for lithium which is estimated to exceed \$100 billion by 2025, is difficult to be met unless alternate recovery techniques are adopted (Natarajan et al., 2019, Meshram et al., 2015). Although the current worldwide lithium reserves amounts to approximately 4 million tonnes, mining activities from solid ores such as lepidolite, spodumene, and montebrasite have been very expensive (Yoshizuka et al., 2002, Chitrakar et al., 2000, Vikstrom et al., 2013, Qi et al., 2017). The recovery of lithium from spent gadgets and batteries is worthy to be considered with respect to optimum resource utilization and the environmental impact caused by the increase in landfills and leaching of toxic metals to the environment.

E-wastes are a promising recyclable source of lithium (Zeng et al., 2014). The total scrap lithium-ion batteries (LIBs) available are estimated to amount to 170,000 tonnes by 2020, out of which lithium coin cells (LCCs) could account for 200–500 tonnes per year (Wang and Wu, 2017, Vanitha and Balasubramanian, 2013). The market for LIBs is expected to rise to \$221 billion by 2024 (Hu et al., 2017, Swain, 2017). As per estimation, 2,50,000 tons of waste LIBs could be generated by electric vehicles sold in 2017 alone (Harper et al., 2019, Lie et al., 2020). As a part of this research, preliminary data collected from three different small-scale e-waste recycling units near the Gandhipuram area in the Coimbatore district, India, revealed electronic items and fitness wearable gadgets as premium recyclable lithium sources in terms of the total LCCs generated. Our data representation revealed the generation of up to 0.01–0.39 tonnes of LCCs (subjected to seasonal variations) from various sources over a duration of one year (1st October 2018–1st October 2019) (Table 1).

Table 1. Quantity of lithium spent coin batteries generated during October 2018-October 2019 from various sources, *Unit I, Unit II and Unit III are small scale e-waste recycling units located in Chinnavedampatti and Gandhipuram, Coimbatore, India.

| Source | Quantity (Tonnes) | | | | | |
|---|---|------------|-------------|--|------------|-------------|
| | 1 st October 2018- 1 st April 2019 | | | 2 nd April 2019-1 st October 2019 | | |
| | Unit I | Unit II | Unit III | Unit I | Unit II | Unit III |
| | Home Appliances (Refrigerator, Washing Machine, Kitchen Blender, Rice Cooker, Microwave Oven) | 0.03 | 0.01 | 0.00 | 0.08 | 0.04 |
| Electronic Equipments System, computer parts, laptops, reading lamps, SD chips) | 0.07 | 0.01 | 0.04 | 0.11 | 0.09 | 0.25 |
| Fitness and Medical (Smart Watches, Medical Gadgets, Blood pressure and glucose monitors) | 0.15 | 0.39 | 0.27 | 0.19 | 0.15 | 0.33 |

Recovery techniques for lithium recovery has been closely studied. Masmoudi et al., combined a chelating agent 3-benzoyl-1,1,1-trifluoroacetone (HBTA) with 1-hexyl-3-methylimidazolium bis(trifluoromethylsulfonyl)imide ionic liquid for selective recovery of lithium (Masmoudi et al., 2021). In order to maintain process sustainability, Chen et al. (2020) introduced a concept of gradient extraction via closed-loop re-fabrication of cathode materials for selective lithium recovery (Chen et al., 2020). Sustainable and simultaneous recovery of lithium and co-ions was attempted from spent ion batteries using tartaric acid as leaching agent and ferro-chemistry approach (Chen et al., 2019, Jiang et al., 2021). Some advancements on recovery techniques include thermal reduction, low temperature pyrolysis, hydrogen roasting, carbonation, double precipitation and mechanochemical approaches. Although scalable, yet these have associated bottlenecks namely, cost of operation, stringent operation conditions and toxicity issues (Table 2). Bio-recovery could thus be an alternative. In our study, we thus identified LCCs as a premier source of lithium and focused on developing a scalable and sustainable technology towards selective recovery from spent cathodes. The environmental impact caused by incorrect disposal of LIBs also justifies the requirement of recycling and recovery (Sethurajan and Gaydardzhiev, 2021). Toxicity leaching tests like Waste Extraction Test (WET), Toxicity Characteristics Leaching Procedure (TCLP) and Total Threshold Limit Concentration (TTLC) analyses revealed that the spent LIBs could be termed as “hazardous” to the environment and leach out toxic metals like Co, Cu, Ni and Pb (Kang et al., 2013).

Table 2. Recent advances on lithium recovery techniques and challenges.

| Technology | Recovery(%) | Time (h) | Interference | Challenges in Scale-Up | Reference |
|---|-------------|----------|----------------|---|------------------------------------|
| Hydro/Pyrometallurgical/Electrochemical | | | | | |
| Separation of Co and Li using polymer inclusion membrane electro dialysis | 99.9 | 10 | Co | Employs ionic liquid which is expensive thus scale up could be non-sustainable | Wang et al., 2022 |
| Thermal reduction of LiCoO ₂ to lithium carbonate and cobalt | 99.96 | <1 | Co | Involves deep eutectic solvent that could be toxic, non-degradable and expensive | Xiao et al., 2021 |
| Low temperature Chlorination Pyrolysis | 99.9 | <1 | Ni, Co Mn | Co-ions are parallelly leached with lithium | Ma et al., 2021 |
| Hydrogen roasting and water leaching to prepare lithium hydroxide | >97 | <1 | Ni, Co,Mn, Al | Hydrogen energy-Expensive and storage issue | Liu et al., 2021 |
| Reduction roasting and carbonation water leaching | 80 | <1 | Co, Mn, Ni | Regulated flow rate of CO ₂ | Zhang et al., 2018 |
| Phosphoric acid based leaching | 87.7 | <1 | Co, Ni, Fe, Mn | Requirement of large volumes of acid in scale-up (30 mL/g) | Chen et al., 2018 |
| Two stage precipitation using Na ₂ CO ₃ and Na ₃ PO ₄ to form LiCO ₃ and LiPO ₄ from recycling waste effluent. These further heat treated with MnCO ₃ to form lithium ion sieves for recovery of lithium | 74-92 | 24 | Na, Ni Mn, Co | Involvement of effluent towards design of the lithium ion sieve could add in unknown ionic impurities that could hinder large scale pure lithium recovery | Guo et al., 2014, Guo et al., 2017 |
| Mechanochemical approach to recover lithium in a hermetic ball to water leach lithium | 99 | <1 | Co | Involves EDTA as co-grinding agen which could raise concerns on toxicity while scale up | Wang et al., 2016 |

Biorecovery

| | | | | | |
|--|-------|----|-----------------------|---|---|
| Granulated $H_4Mn_5O_{12}$/Chitosan for biosorption of lithium from geothermal sources | 88.4 | 48 | Na, K, Ca, Cl^- | No data available on scalable recovery from spent batteries; Research needed on recovery at wide concentration ranges | Ding et al., 2021 |
| Bioleaching of spent lithium ion batteries using sulphur oxidizing or iron oxidizing bacteria | 91 | 48 | Fe | Stringent pH monitoring required the presence of Fe^{3+} which could reduce lithium recovery | Wu et al., 2019 |
| Hybrid system involving biosorption, bioaccumulation and chelation using citric acid and <i>Lysinibacillus sp</i> for lithium recovery from lithium ion batteries | >25% | >1 | Co | Much research needed to establish data on scaling up and associated challenges | (Dolker and Pant, 2019) |
| Imprinted blended chitosan microfibers for recovery lithium from spent LCC cathode leachates | 99.3% | <1 | Co, Ag, Mn, Na, Ca, K | A detailed data on uptake, selectivity and recovery provided as a function of multiple cathodes. We provide a pilot scale analyses for estimation of possible routes and challenges of scale up | This Study |

Bio-recovery techniques for the recovery of value added metals include bio-precipitation, bio-sorption and bio-electrochemical systems. Although being currently implemented, common demerits associated with bio-precipitation include (i) unwanted sludge generation (ii) addition of high loads of chemicals for pH adjustment to attain selective recovery of the desired metals, and (iii) interferences caused by the nutrients and secondary metabolites produced by the microorganisms (Esposito et al., 2006). On the other hand, bio-electrochemical systems involve high capital costs, bio-fouling issues and toxicity to the microorganisms (due to electrode leaching), which limits its application when using real waste leachates (Yang et al., 2019, Zheng et al., 2020). Bio-sorption is recognized as an effective and low cost method for metals recovery from aqueous solutions (Fomina and Gadd, 2014). Apart from affordability and operational simplicity, bio-sorption has few other merits such as possibility for regeneration and generation of lower amount of generated sludge (compared to bio-precipitation). With regards to lithium recovery, the lacunae and scope of research lies in enhancing the biomass stability and surface/chemical modification to prevent early exhaustion of functional groups. The technology is still at an early stage and requires more data in this arena before eventual commercialization.

Chitosan biopolymer has been recognized as an excellent adsorbent for metals, due to its abundant functional groups namely amines and hydroxyls which could avoid early exhaustion of the bio-sorbent (Habiba et al., 2017; Jamshidifard et al., 2019; Monier et al., 2018; Monier et al., 2015). When crosslinked with a suitable agent namely, glutaraldehyde, epichlorohydrin, ethylene glycol diglycidyl ether the biopolymeric matrix develops stability to acidic pH ranges (Qin et al., 2006; Kyzas et al., 2015; Aqil et al., 2015; Laus et al., 2010; Hong et al., 2013). However, selectivity towards the metal of interest amidst the presence of co-ions has been challenging. The imprinting technique has been proven to be quite effective in increasing the selectivity of chitosan matrices to the metal of interest. The technique involves (a) loading chitosan matrix with an ion template which is further crosslinked with a functional reagent (b) removal of metal ion from the polymer matrix to reserve specific binding sites complementary in shape, size, and position to the target metal ion (Fang et al., 2018, He, F. et al., 2019, Yu et al., 2019, Monier et al., 2018). Imprinted chitosan fiber has been employed to selectively recover palladium ions from a multi-metal solution (Mao et al., 2020). Attempts have been made towards the removal of palladium ions using ion imprinted chitosan resin (Monier et al., 2016). Ion-imprinted chitosan chemically modified using amidoxime, diacetylmonoxine, thiol, isatin and melamine-thiourea have been recently reported towards the selective removal of metal ions such as uranyl, nickel, copper, gold and mercury (Elsayed et al., 2021, Elsayed et al., 2021, Elsayed et al., 2020, Monier et al., 2020, Monier et al., 2020, Monier and Abdel-Latif, 2017, Monier et al., 2015). A recent finding suggested that a fibrous and porous adsorbent could be preferable for lithium bio-sorption from brine solution (Wei et al., 2020). In this regard, the importance of the fibrous nature of chitosan membranes was highlighted while fabricating a chitosan nanofiber membrane for the recovery of lithium from a highly concentrated solution (Cheng et al., 2021). This drew our attention towards specific structural aspects (namely swelling ratio and degree of crosslinking) to develop uniquely blended chitosan microfibers which could be further imprinted to selectively recover lithium from spent LCC cathode leachates. Both selective sorption and desorption performances were evaluated in terms of relative lithium sorbed (RLS) and relative lithium released (RLR) for the biorecovery with batch scale and pilot scale approaches. The promising nature of this research has been justified in terms of their scalability and regeneration capacity with minimal adsorbent loss. This research would be very helpful for the readers to gain insights on the significance of blended polymeric matrices in sustainably recovering value added metals from e-waste sources.

2. Materials and methods

The chemicals used in the study have been mentioned in supplementary section 1.0.1.

2.1. Coin cell cathode processing and analyses

Spent coin batteries were procured from an electronic waste recycling unit in Coimbatore, India. Processing was conducted by mechanical followed by chemical process (Chandran et al., 2021). These were immersed in 35% NaCl for a period of 2 days in order to prevent short-circuiting and self-ignition during mechanical opening of the battery. These were opened under expert supervision to recover the electrodes. The electrodes were weighed initially on a physical balance (Ohaus precision balance) and then crushed to obtain particles which were further sieved (sieve size 3 mm) and weighed. The electrode particles (10 g/L) were soaked in 25 mL of HCl solution (2 M) for a period of 60 min. The concentrate was diluted to 1000 mL and filtered using cellulose filters (Whatman grade II; 125 mm diameter; particle retention: 8 μ m) the pH was monitored using a pH meter (Digital pH meter 7007, Digisun Electronics) set-up. Conductivity values were monitored at every 10 min interval using a benchtop conductivity meter (Peak USA T711L Conductivity Meter) (Fig. S5(a)). Instrumental analyses

were performed on 100 mL of leachates. A flame photometer (Flame Photometer 130, compressor unit 126; 230 V, 50 Hz, LPG supported) was employed to analyse lithium, sodium, potassium and calcium. The estimation of cobalt (240.5 nm), manganese (273.7 nm), copper (324.8 nm), nickel (232.0 nm), silver (328.1 nm) and aluminium (396.2 nm) was carried out using an atomic absorption spectrometer (Model: Varian AA-240, Australia; source of ignition: hollow cathode lamp) (Fig. S5(b)).

2.2. Synthesis and characterization of chitosan microfibers

Microfibers were synthesized by blending varied ratios of low (ChA), medium (ChB), and high viscosity (ChC) chitosan. Three variants of chitosan used in this study were pre-characterized for their viscosity, degree of acetylation and particle size. The degree of acetylation (DA) of chitosans was determined by the conductometric method (dos Santos et al., 2009) using a benchtop conductivity meter (Peak USA T711L Conductivity Meter). Viscosities of various blends of chitosan in 0.1 M HCl at 25°C were determined using an Anton Paar rheometer (Model MCR302) with PTFE coated geometries (PP50/CX SN 78925). The values are presented in (Table S1).

Stock solutions of a concentration 10 ± 0.79 mg/mL were prepared by dissolving an appropriate weight of chitosan in 100 mL of 0.1 M HCl, followed by stirring at 1500 rpm at a temperature of 35°C overnight. Following this step, the concentrated stocks were blended appropriately as per the concentrations provided in Tables S3 and S6, filtered via 0.45 μ m and 0.22 μ m syringe filters (Millex), and finally crosslinked by adding a pre-determined volume of glutaraldehyde. The slurries were left overnight on magnetic stirring at 300 rpm. Crosslinking reactions were carried out at 40°C for 2 h (Mao et al., 2020). Microfibers were drawn in 1 M NaOH bath solution by 'continuous injection gelation' technique and cured overnight (Wu et al., 2019). These were dried in a hot air oven at 50°C and stored for further evaluation. The protocol for analyses of swelling ratio (SR) and degree of crosslinking (DC) has been mentioned in supplementary sections 1.0.2 and 1.0.3. Preliminary lithium sorption studies on microfibers were performed to compare the efficacy and determine the optimal blend of chitosan in the microfibers towards the maximum recovery of lithium. Lithium recovery potentials of chitosan were determined as mentioned in supplementary sections 1.0.4. The interactions between chitosan and glutaraldehyde were analyzed using a Box-Behnken design (Design Expert® version 13), predicted values (based on predicted quadratic equations) and model significance has been highlighted in Tables S4, S5, S7 and S8.

Lithium ion-imprinted chitosan microfibers were prepared as per recently established protocols, with modifications (Mao et al., 2020). Blended chitosan (ChA-ChB or ChA-ChC) solutions were prepared in 50 mL of 0.1 M HCl, to which 1% v/v (grade II, 25% purity) glutaraldehyde solution was added for crosslinking. The crosslinked matrix was drawn into fibers in 1 M NaOH bath and soaked in 25 mL of 100 mg/L Li(I) solution for 24 h at 40°C under a stirring rate of 110 rpm. The second set of crosslinking was carried out using 2.5% v/v glutaraldehyde after washing the microfibers several times using de-ionized water. Li(I) loaded matrix was then treated with 0.05 M HCl to remove lithium and create templates on the matrix. The final stage of rinsing and neutralization was carried out using 0.5 M NaOH and de-ionized water. The imprinted matrices were labeled as ChA-ChB(Cr-Li), and ChA-ChC(Cr-Li), dried at 50°C and stored for further analyses.

2.3. Instrumentation

The changes in turbidity were monitored using a digital turbidimeter (Systronic 8966, lower detection limit up to 0.01 NTU). The thermal stability was assessed in an N₂ atmosphere using a thermogravimeter (Perkin Elmer USAA, Diamond) at a temperature range of 50-600°C by an increment of 10°C, post which a differential thermal analysis was performed using GraphPad Prism, version 9.2.0.

The effect of pH on microfiber stability was monitored using a digital pH meter (Digital pH meter 7007, Digisun Electronics) set-up. Values of pH_{pzc}, ion exchange capacity were calculated as per pre-published protocols (Permana et al., 2017, Charumathi and Das, 2012). Functional group and surface topology analyses were performed using a Fourier transform infrared spectroscopy (FTIR) [Schimadzu IR Affinity model] by KBr pellet technique. Scanning electron microscopy (Zeiss Evo 18) and the images were analyzed using an Image J software tool. Surface elemental analyses were performed using an elemental analyzer (Zeiss Evo Smart EDX).

2.4. Lithium recovery studies

2.4.1. Batch adsorption and desorption

Batch adsorption experiments were carried out using imprinted (ChA-ChB(Cr-Li); ChA-ChC(Cr-Li)) and non-imprinted (ChA-ChB(Cr) and ChA-ChC(Cr)) microfibers. The uptake values of lithium and co-ions (Na(I), K(I), Ca(II), Co(II), Mn(II), Ag(I), Al(III), Cu(II), and Ni(II)) was studied in a multi-metal system generated from leachates obtained from n number of cathodes (n = 1–100; ion concentrations and details on weights of dry cathode powder mentioned in Table 3). Experiments were conducted in a working volume of 250 mL at 40°C, pH of 6.1 and 110 rpm in a shaking incubator. Adsorption under above-mentioned conditions was performed at varying time intervals (0–120 min; 10-min interval) and varying biomass dosages (0.1–1.5; 0.1 g interval). Residual metal ions were estimated as mentioned in Section 2.1. The desorption of metal loaded microfibers was carried out by adding 5 g of biosorbent to a working volume of 250 mL of 0.05 M HCl. The pH of the solution was noted to be 2.7. Acid based regeneration was carried out for a period of 6 h under shaking conditions of 110 rpm at 25°C. The adsorption-desorption were conducted for nine cycles. Post desorption, the suspensions were centrifuged at 5000 rpm for 15 min and the supernatant was analysed for residual lithium. The desorption efficiency was studied in terms of relative lithium released which is given as:-

$$\text{Relative Lithium Released (RLR)} = \frac{C_{\text{desorbed Li}}}{C_{\text{Total M}}} \quad (1)$$

Where $C_{\text{desorbed Li}}$ denoted the total desorbed concentration of lithium (mg/L) and $C_{\text{Total M}}$ represents the cumulative concentration of desorbed co-ions.

Table 3. Co-ions present in leachates obtained from powdered cathode materials of LCCs.

| Elements | Concentration Values (mg/L) | | | | |
|-----------|-----------------------------|------------|-------------|--------------|--------------|
| | n=1 | n=5 | n=20 | n=50 | n=100 |
| Lithium | 5.19±0.70 | 30.06±0.71 | 112.16±3.59 | 272.15±10.01 | 491.35±7.96 |
| Cobalt | 0.35±0.09 | 5.25±1.09 | 27.19±0.11 | 44.23±2.09 | 129.17±9.07 |
| Manganese | 1.04±0.76 | 4.97±0.04 | 26.78±4.00 | 68.44±4.76 | 118.82±14.35 |
| Silver | 1.06±0.17 | 8.46±4.33 | 13.37±1.01 | 36.62±7.99 | 54.33±10.19 |
| Aluminium | 0.36±0.17 | 2.19±1.31 | 3.44±0.91 | 7.91±1.33 | 11.06±4.11 |
| Nickel | 0.05±0.01 | 0.17±0.03 | 0.25±0.07 | 1.03±0.07 | 4.11±0.07 |
| Copper | 0.17±0.04 | 0.76±0.09 | 1.33±0.51 | 2.35±0.76 | 2.76±1.39 |
| Sodium | 2.16±1.39 | 12.11±4.09 | 45.16±7.88 | 97.19±13.47 | 201.37±30.31 |
| Potassium | 2.38±1.47 | 16.05±2.06 | 68.15±10.19 | 164.96±23.09 | 326.17±21.99 |
| Calcium | 1.37±0.04 | 8.99±1.15 | 29.19±14.05 | 73.55±11.09 | 135.15±10.01 |

*n represents number of cathodes involved in leachate generation. n=1 cathode (weight of cathode powder: 0.96±0.05 g); n=5 cathodes (weight of cathode powder: 3.96±0.17 g); n=20 cathodes (weight of cathode powder: 18.65±1.06 g); n=50 cathodes (weight of cathode powder: 47.06±0.98 g); n=100 cathodes (weight of cathode powder: 92.35±1.77 g); Leaching conducted using 25 mL of 2 M HCl for 60 minutes on 50 g/L dosage of powdered cathode at 25°C.

2.4.2. Adsorption mechanism and selectivity

Evaluation of equilibrium isotherm constants, kinetic model rate constants, and thermodynamic parameters were performed using a biomass dosage of 1 g/L in a total working volume of 250 mL of cathodic leachates. The leachates were obtained from n cathodes. Here n represents number of cathodes involved in leachate generation (n = 1: weight of cathode powder: 0.96 ± 0.05 g, CoLi: 5.19 ± 0.70 mg/L; n = 5: weight of cathode powder: 3.96 ± 0.17 g, C_{oli}: 30.06 ± 0.71 mg/L; n = 20: weight of cathode powder: 18.65 ± 1.06 g, C_{oli}: 112.16 ± 3.59 mg/L; n = 50: weight of cathode powder: 47.06 ± 0.98 g, C_{oli}: 272.15 ± 10.01 mg/L). In this regard, it would be worthy to mention the contributions of Naseri et al., 2019, who attempted bio-recovery of lithium using bacteria (Naseri et al., 2019). Leachates in this case were derived from whole spent coin cell powder, which had a lithium concentration of 35850 mg/kg. In our study, we considered only powdered spent cathodes as a source to obtain leachates to avoid simultaneous recovery of co-ions along with lithium. Each cathode weighing 0.96 g, the net lithium derived from LCC cathodic leachates was lower than that reported from whole powdered LCCs. The mode of adsorption and maximum adsorption potential of imprinted and non-imprinted microfibers was evaluated on lithium and co-ions using Langmuir and Freundlich isotherms. Constants q_{max} (mg/g) and K_L (L/mg) were determined as per standard equations (Das et al., 2010). Kinetic modelling was performed using pseudo-first, pseudo-second, intraparticle diffusion and Boyd plot models as per standard equations (Das et al., 2012). Equilibrium and kinetic modelling studies were conducted at 40°C. The process spontaneity was assessed using parameters of Gibbs free energy, enthalpy and entropy, (ΔG , ΔH and ΔS respectively), as obtained from standard Eq.(4) and (5) [Das et al. (2015)].

$$\text{Log} \frac{q_e}{C_e} = \frac{\Delta S}{2.303R} - \frac{\Delta H}{2.303RT} \quad (2)$$

$$\Delta G = \Delta H - T\Delta S \quad (3)$$

where q_e/C_e is called the adsorption affinity. The values of ΔH and ΔS were determined from the slope and the intercept of the linear plot of $\log (q_e/C_e)$ vs $1/T$. These values were used to calculate ΔG which is the fundamental criterion of spontaneity. While kinetic and thermodynamic parameters were evaluated for lithium, the microfibers were assessed for their maximum adsorption potential for co-ions namely.

Selectivity parameters namely separation factor (α_M^{Li}) and distribution coefficients (K_d) were estimated to assess the competitive effects of the above-mentioned co-ions on lithium using standard equations (Zhang et al., 2010). Relative lithium sorbed (RLS) was estimated as per the following equation:

$$\text{Relative Lithium Sorbed (RLS)} = \frac{q_e^{Li}}{q_e^M} \quad (4)$$

Where q_e^{Li} and q_e^M represents the equilibrium uptake capacities of the microfibers towards lithium (Li) and Co-ions (M). The experimental conditions were similar to that maintained in case of isotherm parameter assessment.

2.5. Scale up performance

Scale-up performances of non-imprinted and imprinted microfibers on lithium recovery was assessed using a 15 cm glass column with an internal diameter of 3.5 cm. Lithium was adsorbed and recovered from a higher concentration range as compared to that considered for batch studies. Cathodic leachates were derived from a range of 50–250 (n = 50: weight of cathode powder: 47.06 ± 0.98 g, C_{oli} : 272.15 ± 10.01 mg/L; n = 100: weight of cathode powder: 92.35 ± 1.77 g, C_{oli} : 491.35 ± 7.96 mg/L; n = 150: weight of cathode powder: 144.3 ± 1.76 g, C_{oli} : 506.21 ± 7.96 mg/L; n = 200: weight of cathode powder: 192.1 ± 2.55 g, C_{oli} : 573.5 ± 4.99 mg/L; n = 250: weight of cathode powder: 240.6 ± 1.33 g, C_{oli} : 633.61 ± 5.51 mg/L). The set-up was operated using a peristaltic pump in an up-flow mode. An optimum flow rate of 1 mL/min was maintained throughout the study, based on pieces of evidence of previously established reports (Vimala et al., 2011, Charumathi and Das, 2012). Before packing, a net weight of 11.7 ± 1.29 g microfibers (both imprinted and non-imprinted variants) was added to 1 L of cathodic leachates and adsorption studies were conducted at 55 °C and 110 rpm shaking conditions. After 120 min of exposure, the biomass was semi-dried at 40 °C in a hot air oven and packed in the column. Desorption curves for lithium were obtained using 14.3 ± 1.35 g of bio-sorbent and lithium was recovered using 0.05 M of HCl. Based on previously conducted batch experiments, adsorption-desorption cycles 1, 6, and 9 were considered for a comparison between the matrices. A bed depth service time (BDST) analysis was done at bed depths 4 cm (7.6 ± 0.02 g), 8 cm (10.3 ± 1.14 g) and 12 cm (14.3 ± 1.35 g) as per standard equations (Das et al., 2012). The eluent was monitored at an interval of 10 min for recovered lithium, pH, and conductivity.

3. Results and discussion

3.1. Swelling and crosslinking properties

Structural stability of biopolymeric matrix could be achieved by blending with other polymers and chemical crosslinking (Pawar and Yadav, 2014; Pozzo et al., 2019). In this regard, it would be worthy

to mention the contribution of Qin et al., 2021 who developed chitosan reinforced metakaolin-based geopolymer (Qin et al., 2021). The structural aspects of the polymer composite could be attributed to the system viscosity and porosity of chitosan contents. This drew our attention to the fact that probably blending could affect the mechanical properties and further crosslinking to enhance the structural attributes required for the recovery of value-added metals like lithium. Microfibers in the present study have been developed by blending chitosan variants differing in their viscosities (Fig. S1, Table S1). Swelling ratio (SR) (% g/g) and degree of crosslinking (DC) (%) values were found to vary as a function of varying concentration blends of chitosan and glutaraldehyde dosages (Tables S3 and S6). A microfiber containing two different chitosan variants exhibited different surface topological properties when crosslinked with glutaraldehyde (0.55%(v/v)). As shown in Fig. 1(a)-(b), ChA-ChB(Cr) (ChA: 1 mg/mL; ChB: 1 mg/mL) with an average diameter: $496.7 \pm 3.59 \mu\text{m}$, exhibited surface roughness and lacked a distinct porosity, whereas ChA-ChC(Cr) (ChA: 1 mg/mL, ChC: 1 mg/mL) showed a sleek appearance (microfiber diameter: $176.5 \pm 3.44 \mu\text{m}$; pore diameter: $2.29 \pm 0.31 \mu\text{m}$) with uniform porosity. On an overall basis, microfibers synthesized by blending ChA and ChC yielded higher lithium uptake (LU) values (11.30 mg/g) as compared to those synthesized by blending ChA and ChB (9.19 mg/g). Interesting points were noted based on correlations drawn between chitosan blend, DC, SR and LU values. While the increase in concentrations of ChA (3 mg/mL) in the microfiber blend had a limiting effect on LU, central values of ChB (2 mg/mL) and low values of ChC (1 mg/mL) resulted in high LU potential. The blending of low and high viscosity chitosans microfibers resulted in better LU compared to low and medium viscosity chitosan microfibers. Particularly when using 1% glutaraldehyde for crosslinking (Fig. 1(c) and 1(f)). Model significance was suggested by the p-values obtained in ANOVA (Tables S5 and S8). While the interaction between low viscosity chitosan (ChA) and glutaraldehyde played a major role in the case of LU onto the ChA-ChB(Cr) microfibers, all interactions (between chitosans and chitosan-crosslinker) proved their significance in the LU phenomena onto ChA-ChC(Cr) microfibers. The difference in lithium adsorption could thus be attributed to the differences in the degree of crosslinking and swelling ratios. Trends for all three responses are shown in the 3D mesh diagrams by blue, green, and red zones (Figs. S2–S4). A careful inspection of the interactions between chitosans and glutaraldehyde hinted at role played by ChA (in both types of blends) towards LU, thereby suggesting a low-moderate dosage. ChB and ChC dosages were preferred to be moderate and low to obtain matrices preferable for lithium recovery.

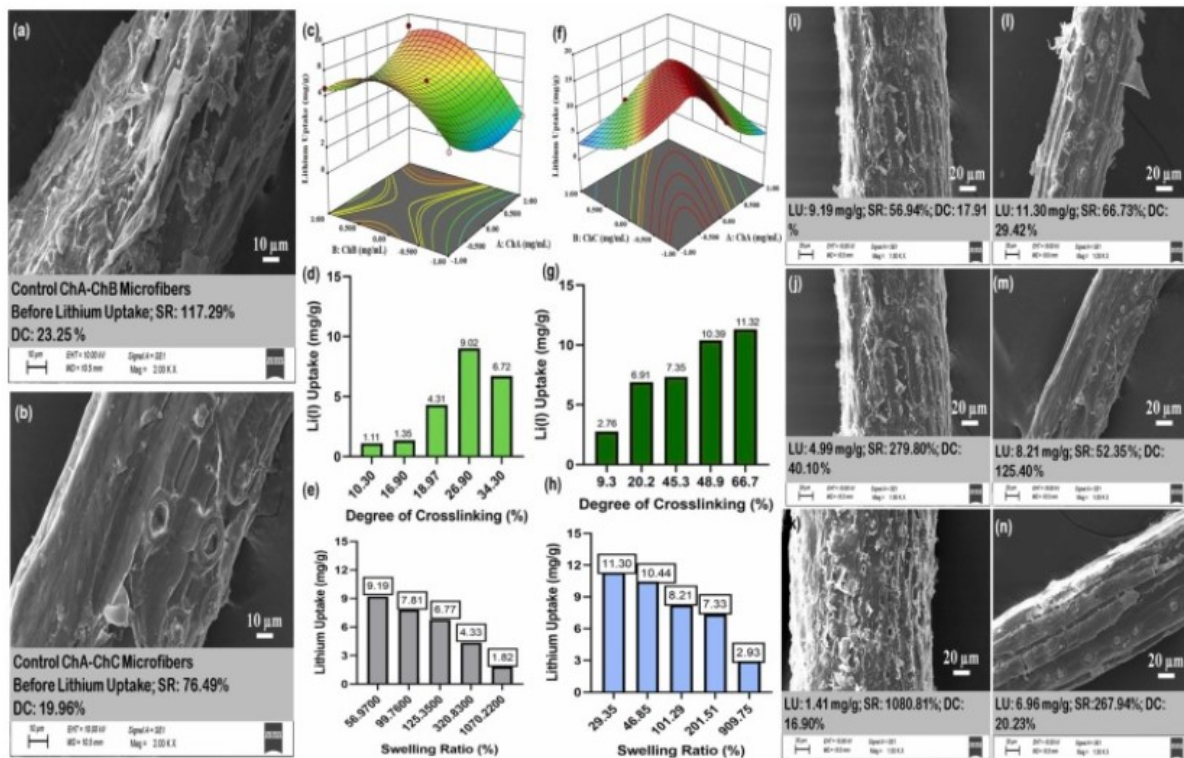


Fig. 1. Correlation between optimal chitosan blends and properties namely, swelling ratio, degree of crosslinking, lithium uptake and surface morphologies. (a) and (b) represent the scanning electron microscopic images of ChA-ChB(Cr) (ChA: 1 mg/mL; ChB: 2 mg/mL) and ChA-ChC(Cr) (ChA: 2 mg/mL; ChC: 1 mg/mL); (c) and (f) represent the 3D mesh diagrams for lithium recovery as a result of interaction between chitosans; Bar graph representations of the effect of swelling ratio and degree of crosslinking on lithium uptake for ChA-ChB(Cr) (Figure (d) and (g)) and ChA-ChC(Cr) (Figure (e) and (h)); Scanning electron microscopy results for ChA-ChB(Cr) microfibers (Figure (i)(j)(k)) and ChA-ChC(Cr) (Figure (l)(m)(n)) after lithium uptake, *Lithium uptake was performed to screen the optimal blend and assess surface features. Experiments were performed in triplicates using 1 g/L biomass dosage in 100 mL working volume of 100 mg/L of LiCl solution, pH 6.1 and shaking speed 110 rpm, contact time: 90 min.

A concise representation of LU as a function of swelling ratio and degree of crosslinking has been represented in Fig. 1(d-h). A direct proportionality between LU and DC was noted in the case of both ChA-ChB(Cr) and ChA-ChC(Cr) microfibers. The optimum level of crosslinking could be determined based on the SR values. A careful analysis suggested DC values of 26.9% (ChA-ChB(Cr)) and 66.7% (ChA-ChC(Cr)) which resulted in low SR values of 56.97% (ChA-ChB(Cr)) and 29.35% (ChA-ChC(Cr)). In this regard, it would be worthy to mention a negative correlation between swelling capacity and heavy metal remediation was previously reported in the case of chitosan/PVA beads (Kumar et al., 2009). Additionally, a tangled shape and structure have also been reported to play a vital role in lithium uptake owing to the prolonged residence time of the ionic solution and the increased specific surface area (Park et al., 2015). In our study, changes in surface morphology have been noticed post uptake of lithium. In this regard, ChA-ChC(Cr) exhibited a high lithium uptake which could be attributed to its slender and porous structure. More compaction was noted post lithium binding (Fig. 1(l): LU: 11.30 ± 2.76 mg/g; diameter: 86.9 ± 1.01 μm; pore size: 1.37 ± 0.33 μm, Fig. 1(m): LU: 8.21 ± 3.99 mg/g; diameter: 87.33 ± 1.35 μm; pore size: 1.26 ± 0.07 μm, Fig. 1(n): LU: 6.96 ± 1.07 mg/g; diameter: 83.21 ± 2.71 μm; pore size: 1.33 ± 0.25 μm). As compared to the control (Fig. 1(a)-(b)), the microfiber diameters were found to decrease post uptake of lithium accompanied by a pore shrinkage, surface protrusions and striations. However, in the case of ChA-ChB(Cr) microfibers, the LU was marked by an increase in surface roughness, whereas, ChA-ChC(Cr) microfibers were marked by an

enhanced porosity (Fig. 1(i) and (m)). Our finding could be correlated to the reports of Ryu et al., who reported the occurrence of internal channels in the lithium manganese oxide-cylinder adsorbents as a result of lithium extraction (Ryu et al., 2016). An interesting fact was that post LU, the swelling ratio remarkably decreased in the case of ChA-ChC(Cr) unlike ChA-ChB(Cr) which suggests that possibly the former could be more stable under varying environmental conditions. However, a crosslinking procedure using glutaraldehyde when performed on chitosan matrix could also enhance its hydrophobicity, which could limit its applications of scalability due to diffusion and mass transfer limitations (Beppu et al., 2007). As a solution to this problem, ion-imprinted bio-sorbents have been recorded to perform better in terms of their enhanced selectivity (Nashad et al., 2012). Moreover, recent reports suggested that the compaction of microfibers could reduce fiber diameters that could enhance lithium adsorption (Choi et al., 2020). A comparison of ion exchange capacities of the non-imprinted and imprinted microfibers in our study suggested imprinting to further enhance the lithium sorption (Table S9).

FT-IR spectra provided us a comparison and clarity on functional groups in non-imprinted, and imprinted forms of microfibers containing optimal blends of ChA-ChB and ChA-ChC (Fig. 2(a)). Least transmittance and broad peak values shown by lithium imprinted microfibers (ChA-ChC(Cr-Li)) at 3441 cm^{-1} suggested higher crosslinking due to interaction between primary amines with C=O moieties of glutaraldehyde. Unlike non-imprinted microfibers, broad peaks were noted for lithium bound microfibers in the range of $3100\text{--}3500\text{ cm}^{-1}$ which could be attributed to the hydrogen bonding between single bond hydroxyl moieties, single bond amine moieties in the chitosan skeleton and the oxygen atom of the carbonyl groups of the glutaraldehyde structure. Very recently, an enhancement in lithium adsorption was attributed to strong intra and inter-hydrogen bonding (O-H) in cellulosic components. This complied with low signals due to C-O stretching and N-H group bending (1110 cm^{-1}) which is in accordance to reports on chitosan which related the stretches between 1095 and 1130 cm^{-1} to the crosslinking of chitosan and glutaraldehyde (Abdeen et al., 2018). A confirmation of glutaraldehyde based crosslinking was indicated by Ndouble bondC peak stretches due to imine groups (1655 cm^{-1}). We could monitor topological changes on the fiber surface and diameter as a result of imprinting (Fig. 2((b)-(e))). Post absorption of water, major difference (5.5 times) was noted in the microfiber diameters for ChA-ChB(Cr) ($496.7 \pm 3.59\text{ }\mu\text{m}$) and ChA-ChC(Cr) ($225.9 \pm 1.57\text{ }\mu\text{m}$) which could be directly correlated with the difference in transmittance intensities of imine stretches. This indicated some interaction between ions and the crosslinking agent. Microfiber diameter values as shown in Table S9 revealed a structural tightening post lithium imprinting. However, the tightening effect was much lesser in case of ChA-ChB(Cr-Li) microfibers ($176.5 \pm 3.44\text{ }\mu\text{m}$) as compared to ChA-ChC(Cr-Li) microfibers ($86.9 \pm 1.01\text{ }\mu\text{m}$). Band characteristics of becoming sharper post migration to lower wavenumbers could be correlated to lithium binding (Abdeen et al., 2018). In this study, we could just draw an inference on the correlation between structural and functional properties as a function of lithium imprinting.

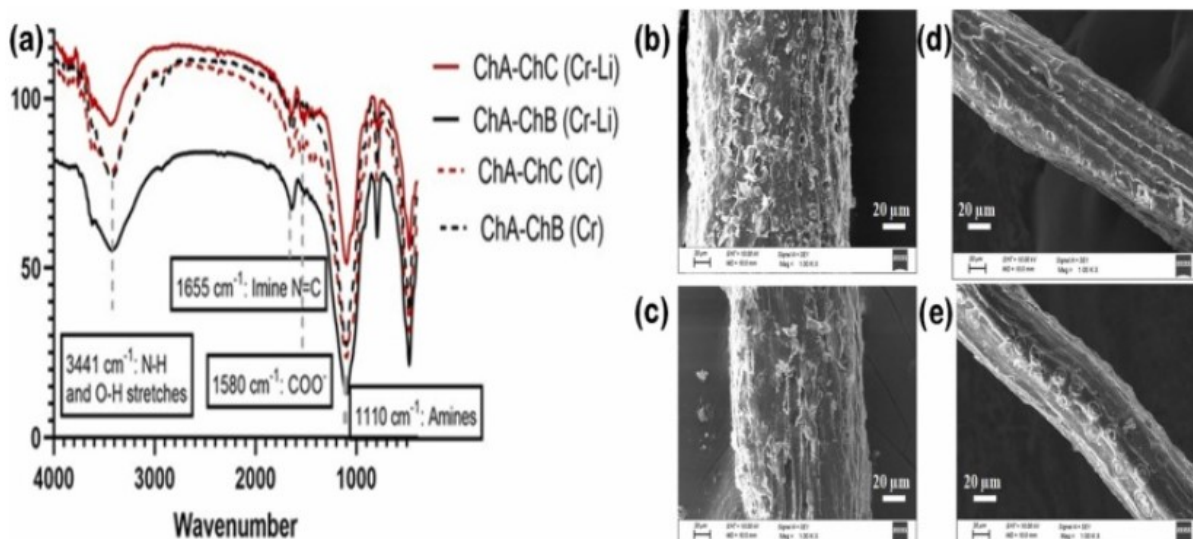


Fig. 2. (a) FT-IR spectra obtained for non-imprinted (ChA-ChB(Cr); ChA-ChC(Cr)) and imprinted (ChA-ChB(Cr-Li); ChA-ChC(Cr-Li)) microfibers; Scanning electron microscopic images of non-imprinted (b)-(c) and imprinted microfibers* (d)-(e), *Microfiber diameter values mention in Table S9.

3.2. Stability analyses

Stability analyses were conducted to understand the impact of lithium imprinting on the enhancement of stability of microfibers in terms of maximum thermal stability and minimal disintegration under pH variations. The study was conducted using microfibers generated from optimal blends of ChA (1 mg/mL) – ChB (2 mg/mL) and ChA (2 mg/mL)-ChC(1 mg/mL). A better understanding was developed by thermogravimetric analyses performed on two variants of microfibers namely non-imprinted (ChA-ChB(Cr); ChA-ChC (Cr)) and Li(I) imprinted (ChA-ChB(Cr-Li); (ChA-ChC(Cr-Li)) microfibers. The TGA and DTA profiles are presented in Fig. 3(a)-(b). The temperature was increased from 25°C to 600°C under the N₂ atmosphere. The weight loss (25-140°C) due to moisture loss in ChA-ChC(Cr-Li) microfibers was ten times less (2.97%) than ChA-ChB(Cr-Li) microfibers (27.69%) which highlighted the relevance of the choice of viscosity in matrix stability. Non- imprinted matrices exhibited higher weight loss during this phase (>60%). The second phase of weight loss was found to occur during 140-370°C, which could be attributed to the breakage of the main chitosan backbone. The decomposition of the fibrous network was found to occur during the third phase of degradation (370-520°C). Based on the data obtained during phases I, II and III, it could be concluded that ChA-ChC(Cr-Li) microfibers exhibited least weight loss (51.76%) as compared to ChA-ChB(Cr)-(82.89%), ChA-ChC(Cr)- 81.99% and ChA-ChB (Cr-Li)- 80.72%. This further accounted for maximum stability due to the dual impacts of crosslinking and imprinting in a fibrous matrix derived from appropriately blended polymers (Zhang et al., 2020). Our research is in accordance with previously reported work on the enhancement of tensile strength of chitosan membranes due to Li(I) binding (Permana et al., 2017).

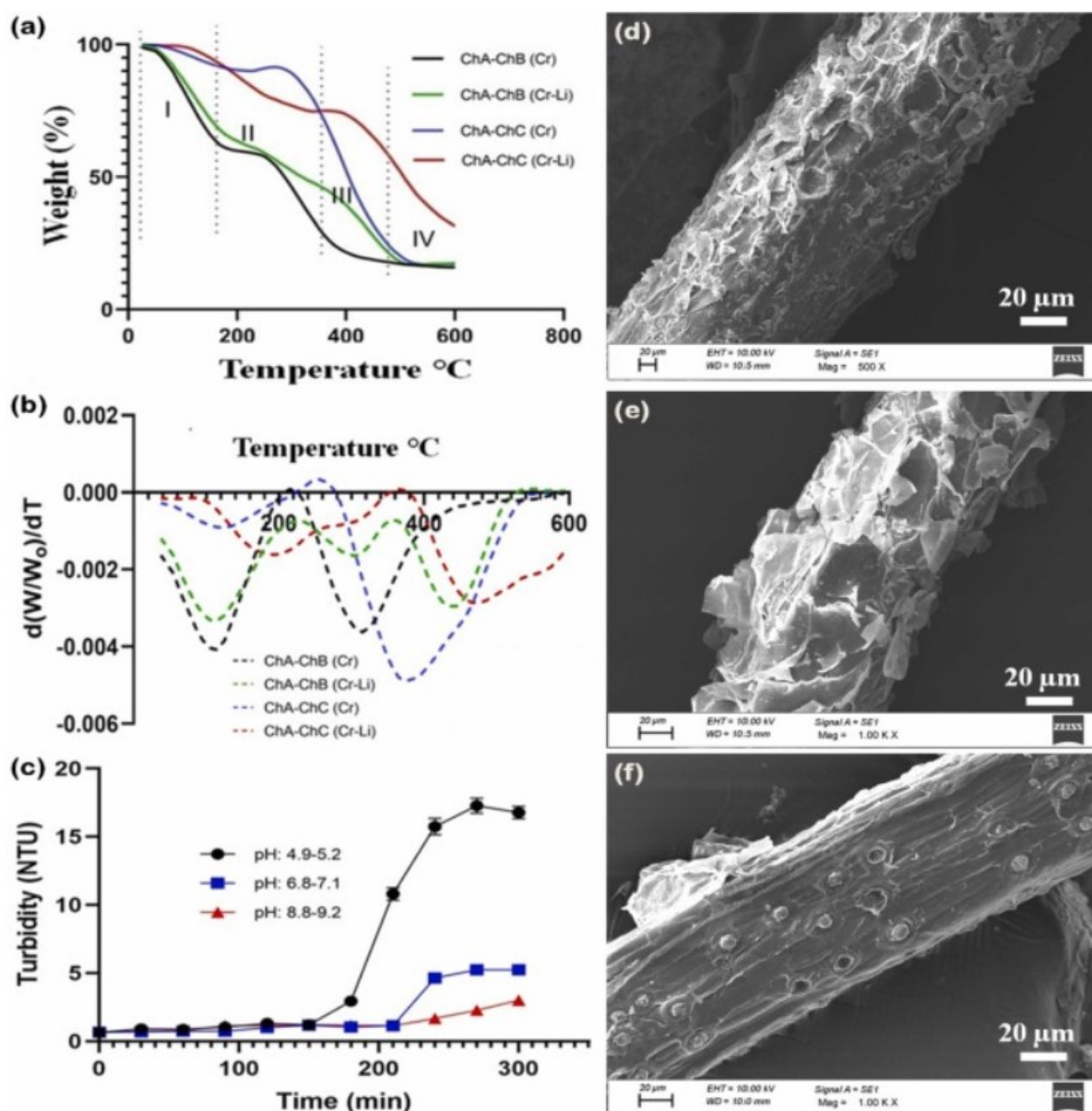


Fig. 3. (a)(b) TGA and DTA curves for non-imprinted and imprinted microfibers (c) turbidity profiles of ChA-ChC(Cr-Li) microfibers at varying pH ranges (d)-(f) Scanning electron microscopic images representing changes in surface morphology of ChA-ChC(Cr-Li) microfibers as a function of acidic, alkaline and neutral pH ranges*, *5 g of ChA-ChC(Cr-Li) microfibers were dipped in 50 mL of acidic, alkaline and neutral pH solutions. Shaking conditions were maintained at 110 rpm at a temperature of 25°C.

The stability of microfibers was further assessed in terms of changes in turbidity as a measure of structural disintegration at acidic, neutral and basic pH ranges (experiments performed in triplicates) (Fig. 3(c)). The increase in turbidity was monitored over a period of 30–300 min. The breakthrough point was noted at the time of an abrupt or a sharp increase in turbidity. In the case of non-imprinted matrices, matrix disintegration and rise in turbidity was noted 45 min onwards (at an acidic pH range), while ChA-ChB(Cr-Li) exhibited stability up to 60 min (data not shown). In the case of ChA-ChC(Cr-Li), a period of 180 min was found to be the breakthrough point after which a slow increase in the turbidity was noted from 1.2 to 17.2 NTU. At neutral and alkaline pH values, a mild breakthrough was noted at 210 min. However, the increase in turbidity was not very significant (from 1.1 to 5.6 NTU). Scanning electron microscopic analyses were conducted after 180 min of exposure to acidic range in order to

examine traces of surface damage, disintegration or swelling. Fig. 3(d)-(f) showed maximum microfiber diameter values of 257.5 μm (acidic pH) followed by 98.87 μm and 98.48 μm at neutral and alkaline ranges, respectively. Although fiber swelling was noted, yet nil fiber disintegration was observed. This was a confirmation of the stability based on fiber swelling and surface damage. Based on the current state of art, it could be thus inferred that the microfibers could remediate heavy metals at concentration ranges between 50 mg/L-100 mg/L at a neutral pH range, without losing its structure (for a contact time of 180 min or longer) (Tang et al., 2020).

3.3. Selectivity and regeneration

3.3.1. Analyses of LCC cathode leachate

Owing to a variety of cathodic material compositions namely, lithium cobalt dioxide (LiCoO_2), lithium manganese oxide (LiMn_2O_4), lithium nickel oxide (LiNiO_2) or lithium vanadium oxide (LiV_2O_3) or in some instances, lithium nickel cobalt complex ($\text{Li}(\text{NiCoMn})\text{O}_2$), the cathode composition could determine the presence of co-ions (Zeng et al., 2014). The concentration of lithium and its co-ions as obtained from 100 mL of acidic leachates from a varying number of cathodes has been represented in Table 3. Data on 5 LCC cathodes (3.96 \pm 0.17 g) has been graphically represented as a function of time for the total lithium concentration (mg/L) and total conductivity (mS) (Fig. S5(a)-(b)). At an equilibrium time of 50 min, the maximum lithium-ion concentration was noted to be 72.33 \pm 11.22 mg/L at an acidic pH of 2.7. Major co-ions included cobalt (15.15 \pm 6.11 mg/L), manganese (27.35 \pm 6.39 mg/L), sodium (34.70 \pm 1.33 mg/L) potassium (50.02 \pm 5.07 mg/L) and calcium (17.25 \pm 10.01 mg/L). Ions at lower concentration ranges included silver (7.33 \pm 3.01 mg/L), nickel (2.15 \pm 0.95 mg/L), copper (1.37 \pm 0.19 mg/L) and aluminium (1.49 \pm 0.80 mg/L).

3.3.2. Competition effects in multi-metal system

We investigated the maximum lithium uptake potential and selectivity of non-imprinted and imprinted forms of microfibers in a diluted leachate solution as a function of input concentrations of lithium obtained by varying the bulk density of cathode powder in leachates. Adsorption experiments were performed at pre-determined biomass dosages and time. Inferences on the sorption performances were drawn from the residual lithium as a function of pH, time and, biomass dosage values (Fig. S6(a)-(c)). An equilibrium time of 60 min was noted to be optimum in the case of non-imprinted and imprinted microfibers. Biomass dosage was not found to have an effect on lithium-bound microfibers and a dosage range of 0.9–1.1 g/L was found to be optimum. A pH value of 6.1 resulted in the least residual lithium values justifying its significance in the present study. On the contrary, lithium recovery was found to be optimum at a pH value of 1.0 and a time period of 80 min in case of lithium ion imprinted membrane (Liu et al., 2020). A detailed comparison of the uptake values of lithium and co-ions has been shown in Tables S10-S13. In the case of all the four variants of microfibers, a steady increase in the lithium uptake was noted till an 'n' value of 50, beyond which the uptake values significantly decreased. The competitive effect plays a significant role in lithium sorption onto biopolymer matrices. The least binding of lithium in a multi-metal system on alginate composite matrices was attributed to interferences from cesium and rubidium ions (Guo et al., 2014). Among all co-ions, cobalt, manganese and silver posed a significant competition in case of non-imprinted matrices. As expected, the uptake of the co-ions was lower in the case of imprinted ones. Precisely, it could be inferred that while manganese could be competitive in the lithium adsorption phenomena onto non-imprinted chitosan microfibers (ChA-ChB(Cr): 16.67 mg/g; ChA-ChC(Cr): 5.81 mg/g), silver was found to be more competitive in case of imprinted microfibers (ChA-ChB(Cr-Li): 10.42 mg/g; ChA-ChC(Cr-Li): 9.174 mg/g). While combinatorial features of surface porosity, roughness and surface charge have been associated with manganese adsorption, the surface adsorption of silver has been

related the surface porosity of a microfibrous matrix (Youngwilai et al., 2020; Freitas et al., 2019). Among the alkaline earth metals, potassium could be highly competitive in case of non-imprinted bio-sorbent, whereas, a moderate competition could be exhibited towards sodium ions in case of imprinted variants.

A closer look at the bound elements provided us with a deeper insight on the co-ion effect in lithium adsorption. EDX analyses of imprinted microfibrers showed stronger lithium peak signals (Atomic weight percentage values: ChA-ChB(Cr-Li): 7.61%, ChA-ChC(Cr-Li): 13.83%) as compared to non-imprinted ones (atomic weight percentage values: ChA-ChB(Cr): 3.17%, ChA-ChC(Cr): 8.01%) (Fig. 4(a)-(d)). The co-ions effect was explained well for ions like silver, manganese, and cobalt. The presence of aluminium peaks on non-imprinted microfibrers was revealed. Recent reports suggested the co-ion hindrance to lithium binding due to aluminium ions (Park et al., 2019, Wahib et al., 2022). This justified low lithium binding on ChA-ChB(Cr) microfibrers (Fig. 4(a)). On the contrary, the fewest bound co-ions are noted in the case of ChA-ChC(Cr-Li) (Fig. 4d). The variations in the binding of co-ions to the adsorbent could be explained in terms their electronegativity, crystal radius and equilibrium constant (Minceva et al., 2008). While the ionic radii of lithium and manganese are similar (0.9 Å), ions like silver and cobalt have ionic radii values of 1.7 Å and 2 Å, respectively.

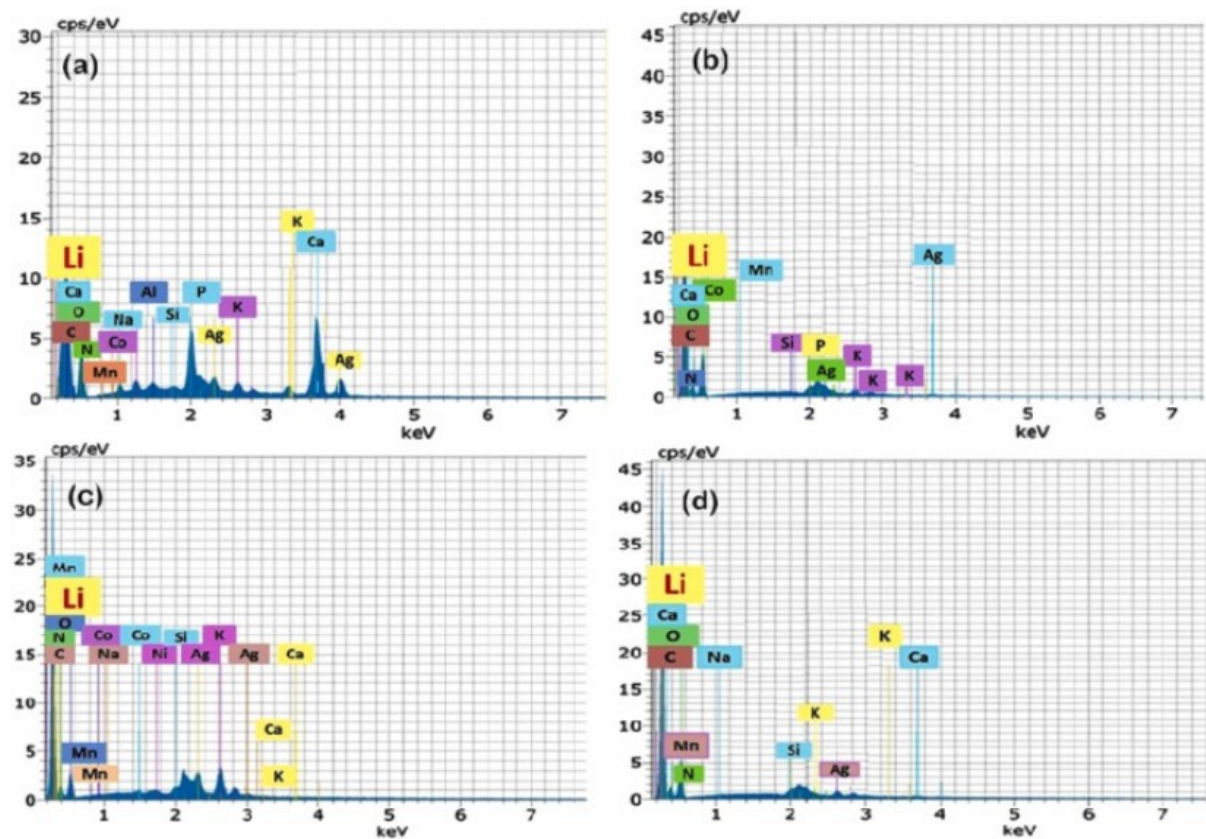


Fig. 4. Energy dispersive X-ray studies showing the binding of co-ions on non-imprinted microfibrers (a)-(b) and imprinted microfibrers (c)-(d)*, *EDX analyses was performed on 0.1 g of biomass samples exposed to 100 mL of cathodic leachates derived from 50 cathodes (Li: 272.15 mg/L, Ag: 36.62 mg/L; Mn: 68.44 mg/L; Co: 44.23 mg/L; Na: 97.19 mg/L; Ca: 73.55 mg/L; K: 164.96 mg/L) at pH 6.1.

Based on the uptake values, the co-ions considered in the present study were silver, manganese, cobalt, sodium, potassium and calcium (Table S10-S13). Relative lithium sorbed (RLS) was estimated as the ratio of lithium uptake to the cumulative uptake of co-ions. The sorption capacity of microfibrers was assessed by exposing them to leachates generated from varying doses of powdered LCC cathodes.

As shown in Fig. 5(a), the value 'n' represents the number of cathodes that could be effectively used as a lithium recovery source. A linear increase in the RLS was noted with an increase in the dosage of lithium. Among the two variants, imprinted microfibers exhibited higher RLS values as compared to non-imprinted ones. ChA-ChC(Cr-Li) microfibers could adsorb up to 25-fold of lithium relatively to other co-ions.

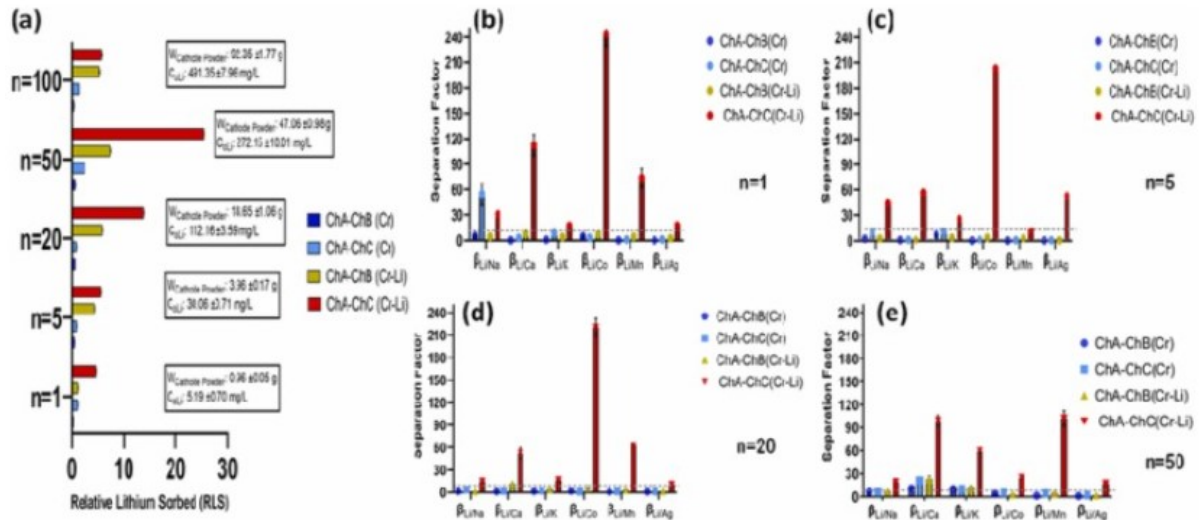


Fig. 5. Estimation of selectivity parameters for lithium onto non-imprinted and imprinted microfibers in a multi-coion system generated from multiple cathodes (a) Grouped analyses of relative lithium sorbed (RLS) onto microfibers in a multi-metal system (b)-(e) Separation factor of lithium estimated as a ratio of lithium and single co-ion uptake values*Experiments to assess selectivity parameters were performed by exposing 1 g/L of biomass to 250 mL of cathodic leachates at pH 6.1, shaking speed of 110 rpm and temperature of 40°C. Leachate details are the same as given in Table 5.

AnAA An abrupt decrease in RLS values was noted at n values of 100. This could be attributed to a phenomenon of 'reversed adsorption' which is could be defined as the repulsion offered by the bound cations in a bio-sorbent framework. This phenomenon has recently been reported in case of phosphonate incorporated metal-organic framework towards its lithium recovery potential due to the repulsion force exerted by cations namely aluminium and copper (Park et al., 2019). As shown in Table 3, aluminium and copper in leachates were noted at concentrations of 7.91 and 2.35 mg/L, respectively. However, in the present study, EDX spectra suggested the binding of cations namely silver, manganese, cobalt and aluminium. Interestingly, the presence of silver, manganese and cobalt was not found to affect the lithium peaks in imprinted matrices, unlike the non-imprinted ones. This could be attributed to different mechanisms of adsorption of each metal according to their physicochemical properties, thereby suggesting that the ion-imprinting technique could possibly overcome the phenomena of reverse adsorption. An illustrative overview is presented in Fig. 6. This could also be justified by the tightened and porous structure of imprinted matrix post lithium binding and imprinting (Fig. 1(l) and Fig. 7(c)). The unique structural features could block the binding of co-ions with higher ionic radii, low charge density and low electrostatic attraction. Low values of RLR obtained in case of ChA-ChB(Cr) suggested the simultaneous release of other co-ions. As estimated, silver (7.65 mg/L), manganese (13.49 mg/L) and cobalt (3.11 mg/L) were released. This implied that non-imprinted blended chitosan microfibers could probably be further investigated to study simultaneous co-ion release. Distribution coefficients as highlighted in Table 4 justified the competitive effects of silver, manganese, cobalt, sodium, potassium and calcium on non-imprinted matrices. In the case of imprinted matrices, the distribution coefficient increased up to 2.7 times and

10.3 times in case of ChA-ChB(Cr-Li) (2733.8 mL/g) and ChA-ChC(Cr-Li) (6969.7 mL/g) respectively. Least effects of co-ions (silver, manganese, sodium and potassium) were noted in case of latter. The results on distribution coefficients of lithium was higher as compared to $H_{1.6}Mn_{1.6}O_4$ based nanofibers, nanofiber sieves employed to recover lithium from sea water (Park et al., 2015, Wei et al., 2020). However, our study would be the first report on the application of imprinted blended chitosan microfibers towards selective recovery of lithium from spent battery powdered cathode leachates.

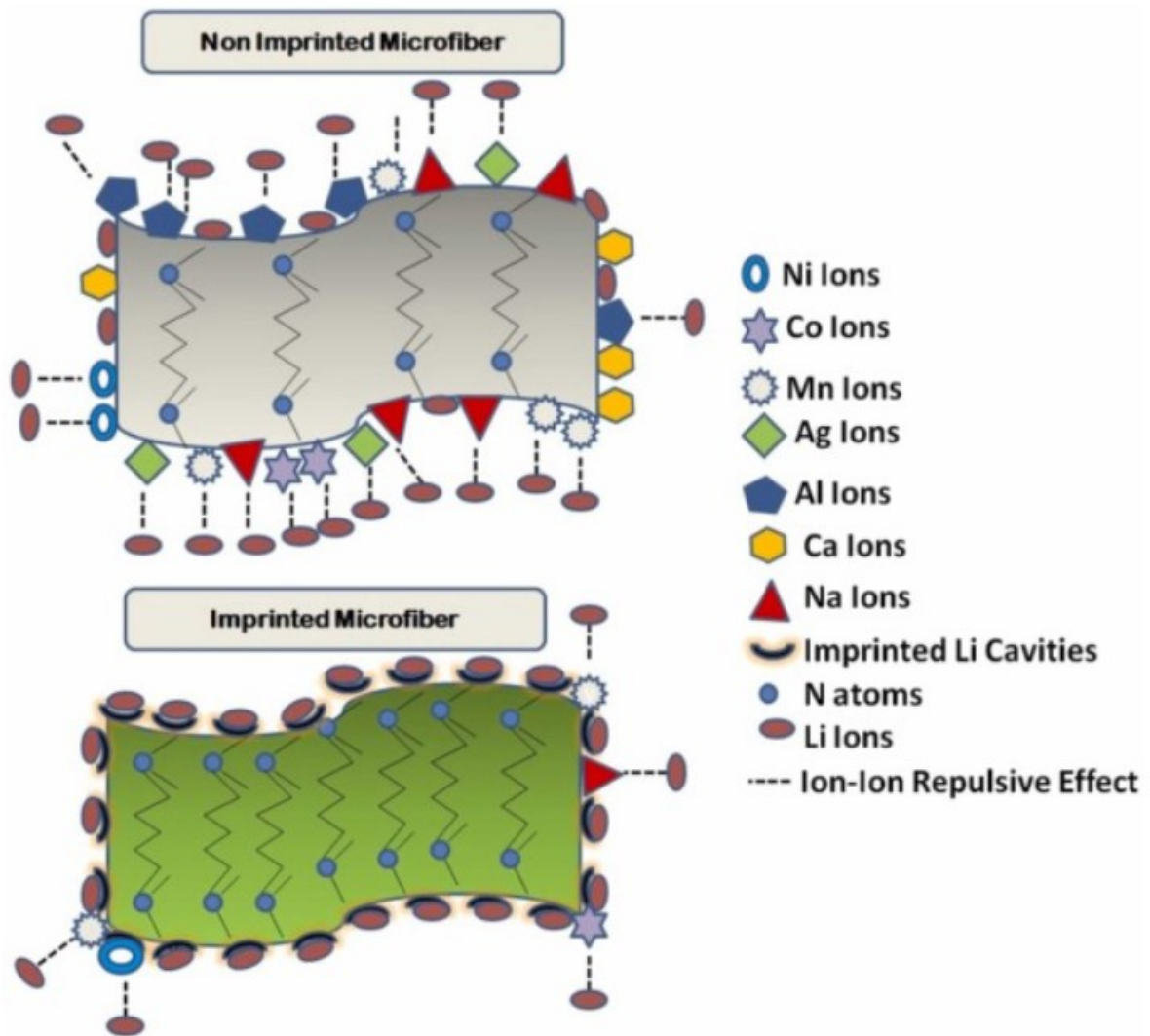


Fig. 6. Illustrative representation showing the binding and repulsive effect of co-ions bound on non-imprinted and imprinted matrices.

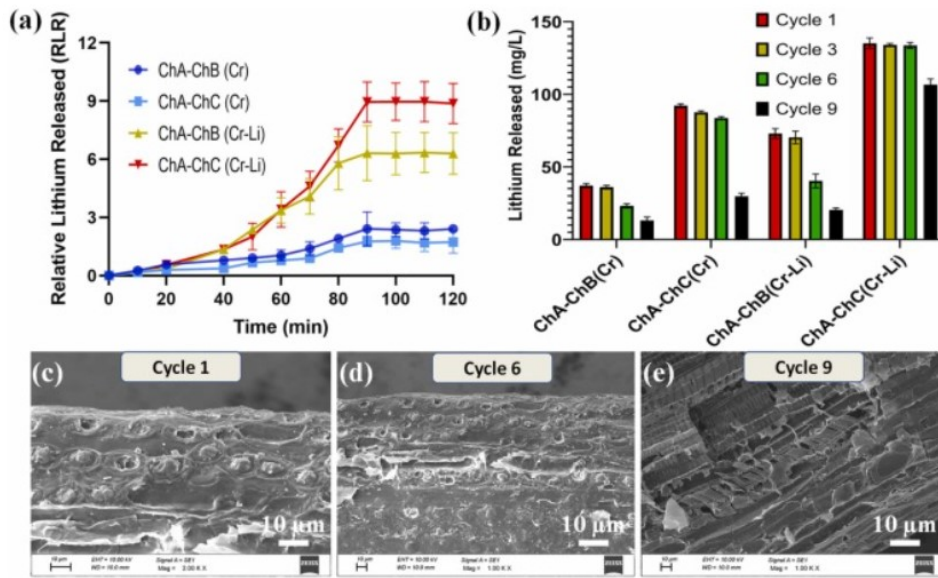


Fig. 7. (a) Selectively desorbed lithium by microfibers (b) regeneration cycles showing the total concentration released* (c)(d)(e) surface topology of ChA-ChC(Cr-Li) microfibers subjected to varying cycles of adsorption-desorption, *Cathodic leachates derived from 50 cathodes containing 272.15 mg/L of lithium; maximum uptake (ChA-ChC(Cr-Li)): 235.4 mg/g; maximum release: 147.9 mg/L; regeneration agent: 0.05 M HCl; desorption time: 12 h; shaking speed: 110 rpm; desorption temperature: 25.1°C

Table 4. Distribution coefficients (mL/g) of lithium and co-ions onto chitosan microfibers.

| Microfiber | n=1 | n=5 | n=20 | n=50 |
|--------------------|--------|--------|-------|-------|
| ChA-ChB(Cr) | | | | |
| Li | 626.9 | 433.5 | 228.1 | 505.3 |
| Ag | 2419.4 | 1424.1 | 286.8 | 580.5 |
| Mn | 2314.8 | 2725.9 | 365.8 | 391.1 |
| Co | 129.0 | 2888.9 | 124.0 | 130.3 |
| Na | 6119.2 | 174.6 | 159.2 | 77.9 |
| K | 692.3 | 56.6 | 151.8 | 49.7 |
| Ca | 2341.5 | 455.9 | 207.7 | 94.9 |
| ChA-ChC(Cr) | | | | |
| Li | 1519.4 | 603.2 | 342.6 | 514.8 |
| Ag | 1255.3 | 944.8 | 298.1 | 254.5 |
| Mn | 1457.8 | 800.7 | 255.5 | 115.4 |
| Co | 481.5 | 422.8 | 348.7 | 101.3 |
| Na | 27.8 | 65.1 | 96.4 | 87.9 |
| K | 182.9 | 51.4 | 147.3 | 73.1 |
| Ca | 505.5 | 495.8 | 164.3 | 63.0 |

| ChA-ChB(Cr-Li) | | | | |
|----------------|--------|--------|--------|--------|
| Li | 2733.8 | 793.6 | 466.9 | 411.2 |
| Ag | 1078.4 | 1668.8 | 315.9 | 213.8 |
| Mn | 625.0 | 258.2 | 149.9 | 91.7 |
| Co | 400.0 | 212.4 | 84.9 | 13.4 |
| Na | 624.1 | 295.2 | 361.5 | 64.2 |
| K | 653.6 | 223.3 | 111.2 | 36.4 |
| Ca | 356.4 | 699.4 | 39.9 | 45.7 |
| ChA-ChC(Cr-Li) | | | | |
| Li | 6969.7 | 2627.8 | 1897.4 | 1713.7 |
| Ag | 394.7 | 206.8 | 177.9 | 100.0 |
| Mn | 94.7 | 239.4 | 30.4 | 16.8 |
| Co | 28.6 | 9.6 | 5.9 | 70.2 |
| Na | 227.3 | 553.2 | 128.7 | 89.7 |
| K | 402.8 | 444.6 | 115.6 | 29.0 |
| Ca | 62.1 | 490.8 | 36.2 | 18.8 |

The separation factor has been reported as a suitable parameter towards specific lithium uptake in a multi-metal ion system comprising of sodium, potassium, rubidium and cesium (Guo et al., 2014). In our study, the selectivity of lithium recovery could be assessed from graphical representations of separation factors (Fig. 5(b)-(e)). An estimate of the separation factor could be beneficial to determine the effect of individual co-ions in a precise way. Grey dotted lines indicated a threshold of 1.00 which signified equal competition between lithium and a co-ion. ChA-ChC(Cr-Li) microfibers exhibited high separation values as compared to other variants. However, sodium, calcium and silver exhibited strong competition effects. Unexpectedly, the separation factors were low ($1 < x < 2$) in case of ChA-ChB(Cr-Li) for all doses of lithium ($n = 1-50$) which signified that the blend of a matrix is vital alongside an imprinting technique to enhance the overall selectivity in ion recovery. In case of ChA-ChC(Cr-Li), the separation factor values although higher than 2, indicated competition from silver, sodium, and potassium ions at cathode dosages of 1, 5, and 50. Selectivity factor values higher than 2 could justify the selective nature of the agent for lithium recovery. In this regard, it could be worthy to mention the selectivity range for lithium-ion imprinted polymers (LIPs) loaded on the surface of multi-wall carbon nanotubes (MWCNTs) (Huang and Wang, 2018). Against co-ions namely potassium, copper and zinc, the selectivity factors were noted to be 3.66, 3.01, 2.05 and 2.10, respectively. Magnetic carbon-based lithium ion-imprinted material exhibited lithium selectivity values of 8.06, 5.72, and 2.75 against sodium, potassium and magnesium (Liang et al., 2020). This data could provide us with a threshold of the minimum input dose of lithium required in a multi-metal system to avoid the phenomena of 'reverse adsorption'. The values obtained in case of ChA-ChC(Cr-Li) were quite similar to the separation factor in case of the applicability of lithium ion sieve nanofiber matrices for recovery of lithium from brine environment (Wei et al., 2020). However, in our study a consistency was maintained even with an increase in the input dosage of lithium which justified the process scalability.

The bio-recovery of lithium was estimated in terms of the relative lithium released (RLR), number of adsorption-desorption cycles and surface texture analyses. Studies were conducted at initial lithium concentrations of 272.15 mg/L obtained from leachates of 50 cathodes (cumulative concentration of co-ions: 484.96 mg/L). The recovery of lithium was found to reach an equilibrium within a period of 90 min. RLR accounts for the ratio of the concentration of desorbed lithium to the total concentration of desorbed co-ions (in this case, ions considered were cobalt, manganese, sodium, potassium, calcium, and silver). The ideal RLR could be expected to be in the range of 9–10 indicating 9–10 times more lithium recovered over co-ion impurities (maximum lithium desorbed: 137.15 mg/L and maximum cumulative concentration of co-ions: <15 mg/L). As shown in Fig. 7(a), maximum RLR values were found to lie close to 9 in case of ChA-ChC(Cr-Li) microfibers. Considerably low values of RLR values of range 1.7–2.5 were exhibited non-imprinted microfibers which exhibited minimal selectivity both in bio-sorption and recovery. The reusability of the fabricated microfibers was investigated over nine cycles and represented as recovery values of lithium from microfiber adsorbent variants over first, third, sixth and ninth cycle of adsorption (Fig. 7(b)). Among the four types, ChA-ChC(Cr-Li) microfibers retained the lithium recovery for up to nine cycles, with a maximum recovery of 137.15 ± 1.31 mg/L. The reduction in recovery is estimated to be less than 20% over the cycles. The ion selectivity of alginate hydrogels and crown ether modified chitosan has been recently reported to maintain lithium adsorption-desorption cycles up to 3–5, respectively (Park et al., 2019, Cheng et al., 2021). In this regard, imprinting of the blended matrix could be a suitable option to recover value-added metals. On a comparative basis, other microfiber variants could maintain the lithium recovery (<100 mg/L; RLR<4) up to 6 cycles. The low reusability of other microfiber types could be attributed to the high binding of alkali metals (sodium and potassium) and alkaline earth metals (calcium) which could cause some structural deformities (Park et al., 2019). The decrease in lithium adsorption has been correlated to changes in fibrous matrix structure leading to aggregation (Choi et al., 2020). A surface topological analysis revealed distinct changes on the surface of ChA-ChC(Cr-Li) microfibers (Fig. 7(c)-(e)). Recent reports on lithium adsorption onto impregnated date pit matrix predicted the formation of various structural complexes based on the size and orientation of adsorbed lithium (Wahib et al., 2022). Chances of penetration from the external surface to the internal pores exist while adsorbing lithium at its higher concentration values. In our study, a decrease in the surface porosity was followed by an enhancement in surface smoothness and further to surface striations which could mark exhaustion of the matrix post aggravated binding of lithium.

3.4. Equilibrium, kinetics and thermodynamics

The non-imprinted and imprinted matrices were analyzed for their mode of lithium binding and process spontaneity as a function of varying lithium concentrations generated from leachates of 1–50 cathodes. The uptake potential of both lithium and co-ions was studied in order to draw parallel inferences on the maximum adsorption capacities of the matrix in a multi-metal system. Langmuir model was used to evaluate the maximum adsorption capacities of lithium and co-ions onto chitosan microfibers. Table 5 represents the isotherm model parameters q_m (mg/g) and K_L (L/mg) along with the correlation coefficient (R²) values. There was a definite increase in the lithium uptake capacities for imprinted fibers (maximum being 100 mg/g in case of ChA-ChC(Cr-Li)) as compared to non-imprinted variants. Our values are quite close to those obtained using date pits impregnated with cellulose nanocrystals and ionic liquid (Wahib et al., 2022). Based on the correlation coefficient values, it could be inferred that the adsorptive recovery of lithium followed a monolayer mode rather than a heterogeneous mode. Our results are in accordance to previously reported literature on lithium sorption on to bio-polymeric matrices (Huang and Wang, 2018, Park et al., 2019, Cheng et al., 2021).

In accordance to the inferences drawn from the concept of 'separation factor' in previous section, Langmuir isotherm could predict the competitive effect of silver and sodium ions in the case of imprinted microfibers. The presence of sodium and its adsorption onto biosorbent has been reported to affect lithium biosorption (Wahib et al., 2022). However, in the case of non-imprinted matrix, a wide range of co-ions (Ag, Mn, Na, K, and Ca) were found to hinder lithium sorption, as indicated by the uptake values. Although attempted, the correlation coefficient values were lesser in the case of Freundlich model (data not shown) which could rule out the possibility of patched or heterogeneous adsorption. The sorption rates were evaluated as a function of both lithium dosage and time using kinetic models namely, Lagergren pseudo-first, pseudo-second, intra-particle diffusion and Boyd plots (Table S14). The main objective was to study the mass transfer mechanism that controlled the adsorption rate. Pseudo-first order was found to exhibit a better fit which suggested the dominance of physisorption over chemisorption in the present study. Fig. S7(a)-(d) shows the model fitting as a function of both lithium dose and type of microfibers. Careful observation showed that the fitting was slightly better at higher input concentrations of lithium ($n = 20$ cathodes and $n = 50$ cathodes). The role of the pseudo-first model has been proven in case of adsorption of transition metal ions on biosorbents. A good fit of pseudo-first order model suggests 'quicker' adsorption unlike the phenomena of chemisorptions (Güzel et al., 2008). The rate of sorption was not found to be affected by the lithium dosage. However, the rate of sorption was found to be lower in the case of imprinted microfibers which could be due to mass transfer limitations. Fig. S7(e)-(h) shows the predominance of a 'two-phased' adsorption in all four types of microfibers. As per Boyd plot a straight line passing through the origin is indicative of sorption processes governed by particle-diffusion mechanisms, otherwise, they are governed by film diffusion (Das et al., 2012). In the present case, although close to the origin, none of the curves obtained were linear straight lines indicative of film diffusion as governing mechanism over intra-particle diffusion (Fig. S7(i)-(l)). This could be beneficial towards the desorption process in terms of time and solvent requirements.

Table 5. Langmuir constants suggesting the maximum uptake potential of microfibers towards lithium and co-ions obtained from cathodic leachates.

| Model | q_{\max} (mg/g) | K_L (L/mg) | R^2 |
|----------------|-------------------|--------------|-------|
| Li | | | |
| ChA-ChB(Cr) | 32.25 | 0.063 | 1.000 |
| ChA-ChC(Cr) | 58.82 | 0.027 | 0.996 |
| ChA-ChB(Cr-Li) | 66.67 | 0.012 | 0.990 |
| ChA-ChC(Cr-Li) | 100 | 0.071 | 0.998 |
| Mn | | | |
| ChA-ChB(Cr) | 16.67 | 0.157 | 0.972 |
| ChA-ChC(Cr) | 5.81 | 0.307 | 0.972 |
| ChA-ChB(Cr-Li) | 3.13 | 0.225 | 0.963 |
| ChA-ChC(Cr-Li) | 6.02 | 0.016 | 0.952 |
| Ag | | | |
| ChA-ChB(Cr) | 6.58 | 0.416 | 0.965 |
| ChA-ChC(Cr) | 6.76 | 0.204 | 0.988 |
| ChA-ChB(Cr-Li) | 10.42 | 0.111 | 0.973 |
| ChA-ChC(Cr-Li) | 9.174 | 0.049 | 0.972 |
| Co | | | |
| ChA-ChB(Cr) | 0.63 | 0.199 | 0.951 |
| ChA-ChC(Cr) | 9.35 | 0.052 | 0.999 |
| ChA-ChB(Cr-Li) | 2.94 | 0.141 | 0.998 |
| ChA-ChC(Cr-Li) | 0.16 | 0.18 | 0.984 |
| Na | | | |
| ChA-ChB(Cr) | 11.36 | 0.010 | 0.995 |
| ChA-ChC(Cr) | 1.09 | 0.024 | 0.992 |
| ChA-ChB(Cr-Li) | 7.58 | 0.001 | 0.981 |
| ChA-ChC(Cr-Li) | 12.19 | 1.000 | 1.000 |
| K | | | |
| ChA-ChB(Cr) | 11.49 | 0.005 | 0.967 |
| ChA-ChC(Cr) | 30.65 | 0.517 | 0.935 |
| ChA-ChB(Cr-Li) | 5.65 | 0.144 | 0.976 |
| ChA-ChC(Cr-Li) | 3.44 | 0.674 | 0.998 |
| Ca | | | |
| ChA-ChB(Cr) | 4.69 | 0.623 | 0.973 |
| ChA-ChC(Cr) | 7.25 | 0.075 | 0.993 |
| ChA-ChB(Cr-Li) | 3.06 | 0.137 | 0.880 |
| ChA-ChC(Cr-Li) | 2.91 | 0.021 | 0.948 |

*. The leachate details are given as:

n=1 (Li: 5.19 mg/L, Ag: 1.06 mg/L; Mn: 1.04 mg/L; Co: 0.35 mg/L; Na: 2.16 mg/L; Ca:1.37 mg/L; K: 2.38 mg/L)

n=5 (Li: 30.06 mg/L, Ag: 8.46 mg/L; Mn: 4.97 mg/L; Co: 5.25 mg/L; Na: 12.11 mg/L; Ca:8.99 mg/L; K: 16.05 mg/L)

n=20 (Li: 112.16 mg/L, Ag: 13.37 mg/L; Mn: 26.78 mg/L; Co: 27.19 mg/L; Na: 45.16 mg/L; Ca:29.19 mg/L; K: 68.15 mg/L)

n=50 (Li: 272.15 mg/L, Ag: 36.62 mg/L; Mn: 68.44 mg/L; Co: 44.23 mg/L; Na: 97.19 mg/L; Ca: 73.55 mg/L; K: 164.96 mg/L)

The process spontaneity was evaluated using thermodynamic parameters namely enthalpy (ΔH), entropy (ΔS) and Gibbs free energy (ΔG) as a function of temperature (25°C, 35°C, 45°C and 55°C) and initial lithium dosage (in terms of the number of cathodes involved). The values are represented in Table 6. While the adsorption phenomena were noted to be endothermic (maximum ΔG value noted to be -20.3 KJ/mol at 55°C) in accordance to the previously established reports (Park et al., 2015), it was interesting to note an increase in randomness at the solid-solution interface when the number of cathodes involved were higher. However, the adsorption spontaneity were found to be purely dependent on the type of microfiber and temperature of adsorption rather than the number of cathodes involved. On a comparative basis, the lithium adsorption onto ChA-ChC(Cr-Li) microfibers was found to be spontaneous (maximum being at an n value of 20). A decrease in spontaneity beyond that could be justified in terms of mass transfer limitations. Table.7.

Table 6. Thermodynamic Parameters as a function of various cathode loads at a varying temperature range.

| n | $\Delta H(\text{KJ/mol})$ | $\Delta S(\text{J/mol K})$ | $\Delta G(\text{KJ/mol})$ | | | |
|----------------|---------------------------|----------------------------|---------------------------|-------|-------|-------|
| | | | 25°C | 35°C | 45°C | 55°C |
| 1 | | | | | | |
| ChA-ChB(Cr) | 19.1 | 60.5 | 1.1 | 0.5 | -0.1 | -0.7 |
| ChA-ChC(Cr) | 25.3 | 22.1 | -1.3 | -2.1 | -3.1 | -3.9 |
| ChA-ChB(Cr-Li) | 16.1 | 44.2 | -1.8 | -2.4 | -2.9 | -3.6 |
| ChA-ChC(Cr-Li) | 73.9 | 7.1 | 1.2 | -1.3 | -3.9 | -6.4 |
| 5 | | | | | | |
| ChA-ChB(Cr) | 8.6 | 89.1 | 2.0 | 1.8 | 1.6 | 1.3 |
| ChA-ChC(Cr) | 7.7 | 21.6 | 1.2 | 1.0 | 0.8 | 0.6 |
| ChA-ChB(Cr-Li) | 16.2 | 54.9 | 0.6 | 1.1 | -0.4 | -0.9 |
| ChA-ChC(Cr-Li) | 100.3 | 43.4 | -9.3 | -12.3 | -16.6 | -20.3 |
| 20 | | | | | | |
| ChA-ChB(Cr) | 16.9 | 60.1 | 3.7 | 3.3 | 2.9 | 2.4 |
| ChA-ChC(Cr) | 19.9 | 52.1 | 3.5 | 2.9 | 2.4 | 1.9 |
| ChA-ChB(Cr-Li) | 17.8 | 53.2 | 1.9 | 1.4 | 0.9 | 0.4 |
| ChA-ChC(Cr-Li) | 56.8 | 85.1 | -4.7 | -6.8 | -8.9 | -10.9 |

| | | | | | | |
|----------------|------|-------|------|------|------|------|
| ChA-ChB(Cr) | 6.6 | 254.2 | 4.5 | 4.4 | 4.4 | 4.2 |
| ChA-ChC(Cr) | 14.6 | 367.8 | 1.6 | 1.2 | 0.8 | 0.3 |
| ChA-ChB(Cr-Li) | 27.7 | 206.3 | 2.3 | 1.5 | 0.7 | -0.2 |
| ChA-ChC(Cr-Li) | 53.1 | 192.1 | -4.2 | -6.1 | -8.0 | -9.9 |

*n represents the number of cathodes involved to obtain the lithium solution.

*For Table 4, Table 5, Table 6: All Experiments were conducted with a biomass dosage of 1.03 g/L, pH: 6.1, stirring rate: 110 rpm, contact time: 90 minutes

Table 7. BDST parameters for estimating maximum column capacity for chitosan microfibers towards bulk recovery of lithium from spent cathodes.

| | n=50 | n=100 | n=150 | n=200 | n=250 |
|-----------------------|----------------------|----------------------|----------------------|----------------------|----------------------|
| ChA-ChB(Cr) | | | | | |
| N | 528.02 | 866.01 | 892.19 | 909.71 | 1116.74 |
| K_a | 3.8×10^{-6} | 2.6×10^{-6} | 5.4×10^{-6} | 2.2×10^{-7} | 5.4×10^{-7} |
| ChA-ChC(Cr) | | | | | |
| N | 720.03 | 1299.01 | 1427.51 | 1617.27 | 1675.11 |
| K_a | 1.4×10^{-5} | 1.2×10^{-5} | 1.6×10^{-5} | 8.8×10^{-6} | 2.2×10^{-5} |
| ChA-ChB(Cr-Li) | | | | | |
| N | 864.03 | 1558.81 | 1605.95 | 1617.27 | 1675.10 |
| K_a | 3.9×10^{-5} | 3.4×10^{-4} | 1.6×10^{-5} | 5.5×10^{-5} | 1.1×10^{-4} |
| ChA-ChC(Cr-Li) | | | | | |
| N | 864.03 | 1558.81 | 1695.17 | 1516.19 | 1340.09 |
| K_a | 4.1×10^{-4} | 2.3×10^{-4} | 2.0×10^{-4} | 1.5×10^{-3} | 1.4×10^{-3} |

*n represents number of cathodes. Flow rate was maintained at 1 mL/min; Total weight of biomass used: 14.3 g

Column volume used: 84.8 cc; Void volume: 21.2 cc; Operational mode: Upward against the gravity

n=50 cathodes (total weight of the cathode powder: 47.1 g, initial lithium concentration: 272.15 mg/L)

n=100 (total weight of the cathode powder: 92.3 g, initial lithium concentration: 491.35 mg/L)

n=150 (total weight of the cathode powder: 144.3 g, initial lithium concentration: 506.21 mg/L)

n=200 (total weight of the cathode powder: 192.1 g, initial lithium concentration: 573.50 mg/L)

n=250 (total weight of the cathode powder: 240.6 g, initial lithium concentration: 633.61 mg/L)

N represents the column capacity (mg/L) and K_a (L/mg min) represents the rate constant

3.5. Scalability analyses

Reusability is an important feature for an adsorbent with respect to the cost of treatment/recovery. Multiple regeneration cycles could reduce the cost of treatment per unit volume of water (Khan and Lo, 2016). Reusability is associated with recovery and stability of the adsorbent (total weight loss 7% during regeneration cycles). The choice of hydrochloric acid as a desorption agent could be attributed to the prevention of the introduction of co-anions in the medium (Lemaire et al., 2014). Our study uses HCl (0.05 M) as the desorption agent as per some reported works (Wahib et al., 2022, Choi et al., 2020, Park et al., 2015, Liu et al., 2021). Packed column processes have been so far employed for large-scale wastewater remediation and allow for large volumes of polluted water to be treated in a short time and these units can be scaled-up from the laboratory to a pilot plant unit where the entire process can be easily controlled (Taha et al., 2016; Chatterjee et al., 2017). Pilot-scale studies were conducted using a packed bed column on non-imprinted and imprinted forms of microfibers individually, to draw an inference on the maximum possible recovery capacity and input dose for a given weight of the sample. Dynamic desorption curves for non-imprinted and lithium imprinted microfibers are represented in Fig. 8. The grey dotted lines represent the breakthrough and exhaustion points. In our study, the parameters considered were (a) ratio of maximum leached lithium concentration to the initial lithium concentration (C_t/C_0) (b) breakthrough period and (c) exhaustion time. All the four microfiber variants were compared based on the mentioned parameters at cycles 1, 6, and 9 respectively. Preferable values for (C_t/C_0) were closer to one since that implied the leached lithium to be almost equal to the supplied lithium. Values less than 1 indicated parallel desorption of other ions namely, silver, calcium and sodium, which could reduce the purity of recovered lithium. A low breakthrough period and an early approach of the exhaustion period were also desirable. In all the cases, a low breakthrough period (less than 90 min) and early approach to exhaustion period (less than 350 min) were noted. Hence the major comparison was drawn based on the C_t/C_0 values. Among the four microfibers, ChA-ChC(Cr-Li) was found to recover maximum lithium with values of 0.991 (cycle 1), 0.997 (cycle 6), and 0.907 (cycle 9). Slightly lower performance was exhibited by ChA-ChB(Cr-Li) with values ranging between 0.7060 and 0.769 over nine cycles. In the case of non-imprinted fibers, although the lithium recovery was maintained during the first cycle (ChA-ChB(Cr)– 0.759; ChA-ChC(Cr)– 0.899), the recovery was found to decrease over the 6th and 9th cycles. Based on the exhaustion period, bed depth service time (BDST) analyses was performed at bed depths 4 cm, 8 cm and 12 cm respectively. The service time considered here was the duration required to reach exhaustion and achieve maximum values of C_t/C_0 . Steep curves were maintained for all the four microfiber variants during the first cycle which implied a short breakthrough and a quick approach of exhaustion (Vimala et al., 2011). However, the steepness of the curve was found to reduce in the case of ChA-ChB(Cr) and ChA-ChC(Cr) microfibers which could be attributed to low values of C_t/C_0 ratio. In this regard, it could be worthy to mention that the column capacity values were found to be higher in the case of ChA-ChB(Cr-Li) and ChA-ChC(Cr-Li) microfibers as compared to the non-imprinted variants. The rate constant values were maximum in the case of ChA-ChC(Cr-Li) microfibers (Table S14). An increase in the rate constant values were noted as a function of the initial lithium concentration, which in turn depended on the number of cathodes recycled. Larger values of rate constant signified that in the case of ChA-ChC(Cr-Li) microfibers, shorter beds could lead to faster lithium recovery and a quick approach in the exhaustion time. On the contrary, non-imprinted microfibers exhibited the requirement of longer beds for this process. The requirement of short periods for lithium recovery has been reported in our study in accordance to recent reports on lithium recovery using LIS-HEC-40 cryogel (Liu et al., 2021). The time period required for lithium recovery were lesser than the values reported in previous studies, which were 12 h (Hong et al., 2013, Nisola, G.M. et al., 2015, Ryu et al., 2016, Ryu et al., 2017). The shorter period requirement for lithium recovery could be associated with

the performance efficiency of the microfibers in terms of the intra-particle and film diffusion patterns due to the surface topological variations. As discussed in the previous sections, film diffusion predominantly governs the lithium adsorption process which could result in shorter periods of adsorption-desorption cycles.

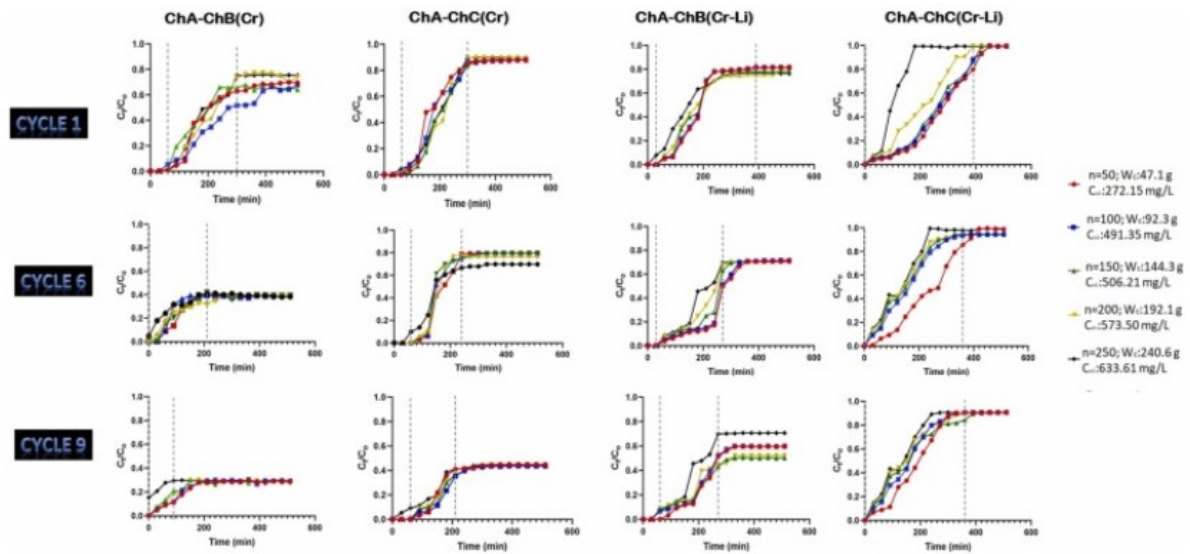


Fig. 8. Desorption curves obtained from packed bed column studies to estimate the scale up potential of microfibers towards recovery of lithium from cathodic leachates obtained at a bulk scale*, *Total weight of adsorbent used: 14.3 g; flow rate: 1 mL/min, pH of recovered lithium solution: 2.7; bed height: 12 cm; breakthrough period overcome within 90 min; exhaustion period reached in 350 min.

A concise summary of this technique of recovering lithium has been represented as a flow chart (Fig. 9). The applicability of ion-imprinted blended bio-polymeric matrices could be an appropriate choice towards recovering lithium from spent cathode leachates. The flow chart highlights that lithium recovery from a diverse concentration range using 10 times lesser solvent concentrations than usually required for desorption. The process also abrogates the need of harmful solvents and additional energy which justifies its cost and energy efficiency.

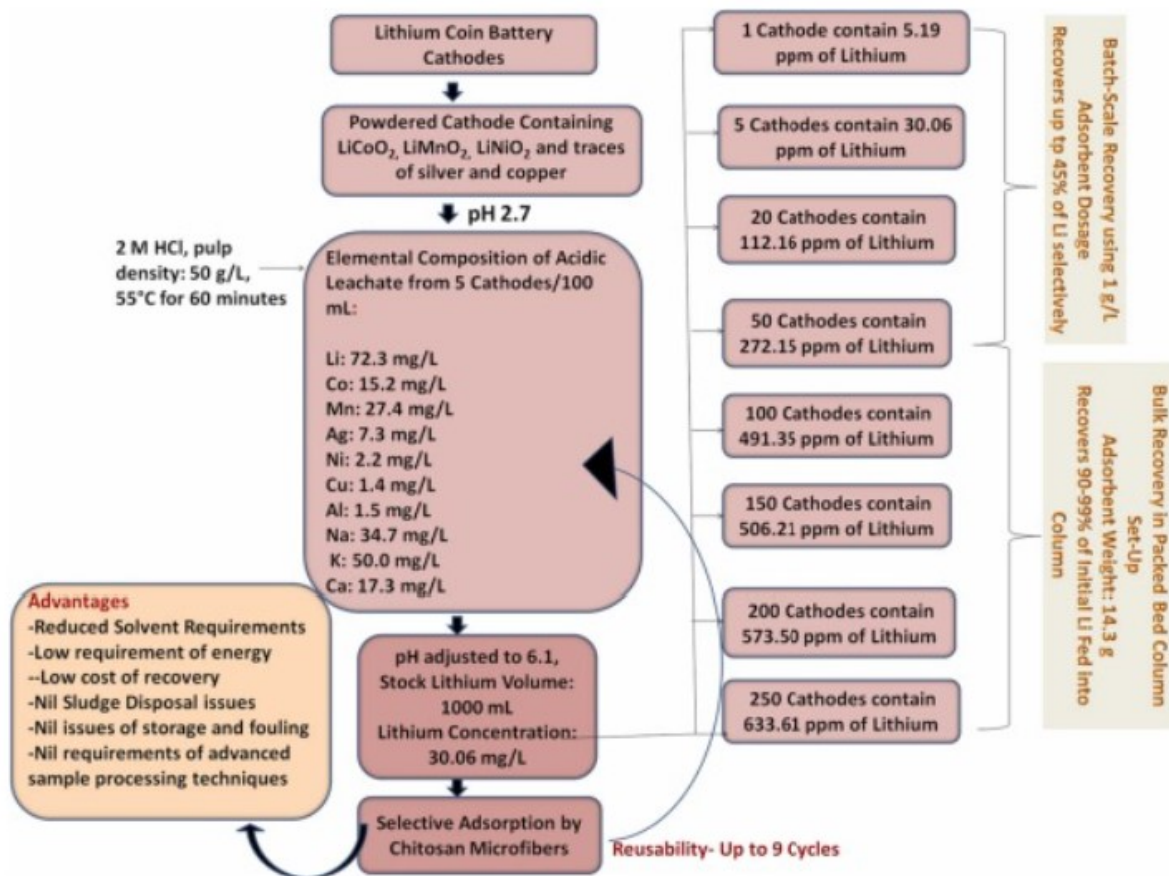


Fig. 9. Flow Diagrammatic representation briefly depicting the lithium recovery phenomena, scalability and advantages using chitosan microfiber matrix.

4. Conclusion

In the present study, we fabricated uniquely blended and crosslinked chitosan microfibers by continuous injection gelation to examine their feasibility to recover lithium from multi-metal solution (derived from cathodic leachates) at batch and pilot scale. Lithium sorption and recovery were correlated to the structural attributes namely, swelling ratio and degree of crosslinking. The core findings are outlined as follows:

- Blends of low (ChA), moderate (ChB) and high viscosity (ChC) chitosans could generate two types of microfibers with unique structural properties (ChA-ChB(Cr): microfiber diameter: $496.7 \pm 3.59 \mu\text{m}$, exhibited surface roughness and lacked a distinct porosity, Li(I) uptake: 9.2 mg/g; ChA-ChC(Cr): microfiber diameter: $176.5 \pm 3.44 \mu\text{m}$, pore diameter: $2.29 \pm 0.31 \mu\text{m}$, Li(I) uptake: 11.3 mg/g).
- Surface Li-ion imprinting imparted noticeable properties like enhanced surface porosity (diameter: $83.21 \pm 2.71 \mu\text{m}$; pore size: $1.33 \pm 0.25 \mu\text{m}$), thermal stability (ChA-ChC(Cr-Li) microfibers exhibited least weight loss (51.76%) as compared to ChA-ChB(Cr)-(82.89%), ChA-ChC(Cr)- 81.99% and ChA-ChB (Cr-Li)- 80.72%), selectivity (K_D : 6969.7 mL/g, α_{M}^{Li} : >90, RLS: >20, RLR: 9) and improved regeneration ability (Recovery up to 99.1% lithium up to 9 cycles).
- Scalability of the process was justified since a total dosage of 14.3 g could recover 99.1% lithium using 0.05 M HCl in a packed bed column (column capacity: 864.03 mg/L) up to 9 regeneration cycles with least material loss (<7%). Steep breakthrough curves were obtained with a quick approach to the exhaustion period implying a quick recovery

Perspective

The bio-sorbent developed in the present study was quite at par with inorganic matrices, and lithium manganese oxides that are used for lithium recovery to date. However, in terms of reduced material loss and high scalability, this could serve as a potential matrix to recover lithium from e-waste sources. As an alternate strategy to pyrometallurgy, hydrometallurgy, chemical-biological hybrid systems and microbe-based leaching processes, this strategy is energy efficient, requires low solvent, time-efficient, easily operable and involves nil expensive storage techniques. This study is an advanced step taken to identify suitable, sustainable and scalable bio-recovery techniques for recovering lithium ions from cathodic leachates.

Author contribution

Dr. Devlina Das conceived the research idea, designed and performed the experiments and framed the manuscript. Ms. Abarajitha R collected relevant literature and data and performed preliminary analyses. Prof. Nilanjana Das (Mitra) provided her extensive supervision, guidance and equipment support throughout the entire project duration. Prof. V. Ramamurthy provided his valuable supervision in developing, implementing the concept of lithium recovery, manuscript reviewing and editing. Prof. Francisco M. Goycoolea, an expert in biopolymers, provided his supportive guidance on the rheological characterization of chitosan, concept development, manuscript reviewing and editing. Prof. Paul Kay being an expert in the field of water science provided his valuable input to improve the overall quality of the manuscript by reviewing and editing.

CRedit authorship contribution statement

Devlina Das (Principal Investigator): Conceptualization, Supervision, Investigation, Writing – review & editing. Abarajitha Ravi: Investigation, Preliminary analyses. Paul Kay: Writing – review & editing. V. Ramamurthy: Conceptualization, Supervision, Writing – review & editing. Francisco Goycoolea: Conceptualization, Supervision, Writing – review & editing. Nilanjana Das: Conceptualization, Supervision, Investigation, Writing – review & editing.

Declaration of Competing Interest

The authors declare that they have no known competing financial interests or personal relationships that could have appeared to influence the work reported in this paper.

Acknowledgement

The presented work has been funded by the Biotechnology Industry Research Assistance Council (BIRAC) (Biotechnology Ignition Grant (BIG) Call 11), Department of Biotechnology, Govt. of India (Grant Number: BIRAC/IKP0536/BIG-11/17), in partnership with IKP Knowledge Park, Telangana – 500101, India and incubation support of PSG-STEP, Coimbatore-641004, India. The research has been independently carried out at the Bioremediation Laboratory, School of Biosciences and Technology, Vellore Institute of Technology (Katpadi, Vellore-632014, India), Department of Biotechnology, PSG College of Technology, (Coimbatore-641004, India) and School of Food Science and Nutrition, University of Leeds (Leeds, United Kingdom, LS2 9JT). We acknowledge PSG College of Technology (Department of Biotechnology), PSG Institute of Advanced Studies (PSG-IAS), PSG-STEP (Coimbatore-641004, India), Vellore Institute of Technology (Bioremediation Laboratory, School of Biosciences and Technology), sophisticated analytical instrument facility (SAIF) IIT Bombay (Mumbai-400076, India),

and the School of Food Science and Nutrition, University of Leeds (LS2 9JT, United Kingdom) for instrumentation and incubation support.

Reason for consideration

We focus on resource recovery from e-waste leachates using bio-recovery technique. Available data on hazards associated with heavy metal leaching from e-wastes necessitates the recovery and remediation.

Appendix A. Supplementary material

References

Abdeen,Z.I, Farargy,A.F.El, N.A. Negm

Nanocomposite framework of chitosan/polyvinyl alcohol/ZnO: preparation, characterization, swelling and antimicrobial evaluation

J. Mol. Liq., 250 (2018), pp. 335-343

A. Aqil, V.T. Tchemtchoua, A. Colige, G. Atanasova, Y. Poumay, C. Jerome

Preparation and characterizations of EGDE crosslinked chitosan electrospun membranes

Clin. Hemorheol. Micro, 60 (2015), pp. 39-50

M.M. Beppu, R.S. Vieira, C.G. Aimoli, C.C. Santana

Crosslinking of chitosan membranes using glutaraldehyde: effect on ion permeability and water absorption

J. Mem. Sci., 301 (1–2) (2007), pp. 126-130

V. Chandran, A. Ghosh, C.K. Patil, V. Mohanavel, A.K. Priya, R.R.R. Madavan, U. Muthuraman, A. Kart hick

Comprehensive review on recycling of spent lithium-ion batteries

Mat. Today Proc., 47 (1) (2021), pp. 167-180

D. Charumathi, N. Das

Packed bed column studies for the removal of synthetic dyes from textile wastewater using immobilised dead *C. tropicalis*

Desalination, 285 (2012), pp. 22-30

S. Chatterjee, Sivareddy,I, De,S

Adsorptive removal of potentially toxic metals (cadmium, copper, nickel and zinc) by chemically treated laterite: single and multicomponent batch and column study

J. Environ. Chem. Eng., 5 (2017), pp. 3273-3289

X. Chen, L. Cao, D. Kang, J. Li, T. Zhou, H. Ma

Recovery of valuable metals from mixed types of spent lithium ion batteries. Part II: selective extraction of lithium

Waste Manag., 80 (2018), pp. 198-210

X. Chen, D. Kang, L. Cao, J. Li, T. Zhou, H. Ma

Separation and recovery of valuable metals from spent lithium ion batteries: simultaneous recovery of Li and Co in a single step

Separ. Purif. Technol., 210 (2019), pp. 690-697

X. Chen, D. Kang, J. Li, T. Zhou, H. Ma

Gradient and facile extraction of valuable metals from spent lithium ion batteries for new cathode materials re-fabrication

J. Hazard. Mater., 389 (2020), Article 121887

Q. Cheng, Y. Zhang, X. Zheng, Li Sun, W. B. Wang, D. Z. Zhongyu Li

High specific surface crown ether modified chitosan nanofiber membrane by low-temperature phase separation for efficient selective adsorption of lithium

Sep. Purif. Technol., 262 (2021), Article 118312

R. Chitrakar, H. Kanoh, Y. Miyai, K. Ooi

A new type of manganese oxide ($\text{MnO}_2 \cdot 0.5\text{H}_2\text{O}$) derived from $\text{Li}_{1.6}\text{Mn}_{1.6}\text{O}_4$ and its lithium ion-sieve properties

Chem. Mater., 12 (2000), pp. 3151-3157

S. Choi, G. Hwang, S. Ilyas, Y. Han, N.V. Myung, B. Lee, Y. Song, Hyunjung Kim, H

Inorganic nanofiber as a promising sorbent for lithium recovery

Sep. Purif. Technol., 242 (2020), Article 116757

D. Das, N. Das, L. Mathew

Kinetics, equilibrium and thermodynamic studies on biosorption of Ag(I) from aqueous solution by macrofungus *Pleurotus platypus*

J. Hazard. Mater., 184 (1–3) (2010), pp. 765-774

D. Das, G. Basak, V. Lakshmi, N. Das

Kinetics and equilibrium studies on removal of zinc(II) by untreated and anionic surfactant treated dead biomass of yeast: batch and column mode

Biochem. Eng. J., 64 (2012), pp. 30-47

D. Das, R. Vimala, N. Das

Removal of Ag(I) and Zn(II) ions from single and binary solution using sulfonated form of gum arabic-powdered mushroom composite hollow semispheres: Equilibrium, kinetic, thermodynamic and ex-situ studies

Ecol. Eng., 75 (2015), pp. 116-122

W. Ding, J. Zhang, Y. Liu, Y. Guo, T. Deng, X. Yu

Synthesis of granulated $H_4Mn_5O_{12}$ /chitosan with improved stability by a novel cross-linking strategy for lithium adsorption from aqueous solutions

Chem. Eng. J., 426 (2021), Article 131689

T. Dolker, D. Pant

Chemical-biological hybrid systems for the metal recovery from waste lithium ion battery

J. Environ. Manag., 248 (2019), Article 109270

Z.M. dos Santos, A.L.P.F. Caroni, M.R. Pereira, D.R. da Silva, J.L.C. Fonseca

Determination of deacetylation degree of chitosan: a comparison between conductometric titration and CHN elemental analysis

Carbohydr. Res., 344 (18) (2009), pp. 2591-2595

N.H. Elsayed, A. Alatawi, M. Monier

Diacetylmonoxime modified chitosan derived ion-imprinted polymer for selective solid-phase extraction of nickel (II) ions

React. Funct. Polym., 151 (2020), Article 104570

N.H. Elsayed, M. Monier, R.A.S. Alatawi

Thiosemicarbazide-modified/ion-imprinted phenolic resin for selective uptake of cadmium ions

Mater. Chem. Phys., 264 (2021), Article 124433

N.H. Elsayed, R.A.S. Alatawi, M. Monier

Amidoxime modified chitosan based ion-imprinted polymer for selective removal of uranyl ions

Carbohydr. Polym., 256 (2021), Article 117509

G. Esposito, A. Veeken, J. Weijma, P.N.L. Lens

Use of biogenic sulfide for ZnS precipitation

Separat. Purif. Tech., 51 (1) (2006), pp. 31-39

L. Fang, X. Min, R. Kang, H. Yu, S.G. Pavlostathis, X. Luo

Development of an anion imprinted polymer for high and selective removal of arsenite from wastewater

Sci. Total Environ., 639 (2018), pp. 110-117

M. Fomina, G. Gadd

Biosorption: current perspectives on concept, definition and application

Bioresour. Tech., 160 (2014), pp. 3-14

G.R. Freitas de, M.G.A. Vieira, M.G.C. da Silva

Fixed bed biosorption of silver and investigation of functional groups on acidified biosorbent from algae biomass

Environ. Sci. Pollut. Res. Int, 36 (2019), pp. 36354-36366

T. Guo, Y. Hu, X. Gao, X. Ye, H. Liu, Z. Wu

Competitive adsorption of Li, Na, K, Rb and Cs ions onto calcium alginate–potassium tetraphenylborate composite adsorbent

RSC Adv., 4 (2014), pp. 24067-24072

X. Guo, X. Cao, G. Huang, Q. Tian, H. Sun

Recovery of lithium from the effluent obtained in the process of spent lithium-ion batteries recycling

J. Environ. Manag., 198 (2017), pp. 84-89

F. Güzel, H. Yakut, G. Topal

Determination of kinetic and equilibrium parameters of the batch adsorption of Mn (II), Co (II), Ni (II) and Cu (II) from aqueous solution by black carrot (*Daucus carota* L.) residues

J. Hazard. Mater., 153 (3) (2008), pp. 1275-1287

U. Habiba, A.M. Afifi, A. Salleh, B.C. Ang

Chitosan/(polyvinyl alcohol)/zeolite electrospun composite nanofibrous membrane for adsorption of Cr⁶⁺, Fe³⁺ and Ni²⁺

J. Hazard. Mater., 322 (2017), pp. 182-194

G. Harper, R. Sommerville, E. Kendrick, L. Driscoll, P. Slater, R. Stolkin, A. Walton, P. Christensen, O. Heidrich, S. Lambert, A. Abbott

Recycling lithium-ion batteries from electric vehicles

Nature, 575 (7781) (2019), pp. 75-86

Z. He, F. Song Lu, Z. M., X. Liu, X. P. Tang, H. Huo, P., *et al.*

Selective reduction of Cu²⁺ with simultaneous degradation of tetracycline by the dual channels ion imprinted POPD-CoFe₂O₄ heterojunction photocatalyst

Chem. Eng. J., 360 (2019), pp. 750-761

H.J. Hong, I.S. Park, T. Ryu, T. Kim Ryu, J. B.G, K.S. Chung

Granulation of Li_{1.33}Mn_{1.67}O₄ (LMO) through the use of cross-linked chitosan for the effective recovery of Li⁺ from seawater

Chem. Eng. J., 234 (2013), pp. 16-22

J. Hu, J. Zhang, H. Li, Y. Chen, C. Wang

A promising approach for the recovery of high value-added metals from spent lithium-ion batteries

J. Power Sources, 351 (2017), pp. 192-199

Y. Huang, R. Wang

An efficient lithium ion imprinted adsorbent using multi-wall carbon nanotubes as support to recover lithium from water

J. Clean. Prod., 205 (2018), pp. 201-209

S. Jamshidifard, S. Koushkbaghi, S. Hosseini, S. Rezaei, A. Karamipour, A. Jafari rad

Incorporation of UiO-66-NH₂ MOF into the PAN/chitosan nanofibers for adsorption and membrane filtration of Pb(II), Cd(II) and Cr(VI) ions from aqueous solutions

J. Hazard Mater., 368 (2019), pp. 10-20

Y. Jiang, X. Chen, S. Yan, S. Li, T. Zhou

Pursuing green and efficient process towards recycling of different metals from spent lithium-ion batteries through Ferro-chemistry

Chem. Eng. J., 426 (2021), Article 131637

D.H.P. Kang, M. Chen, O.A. Ogunseitan

Potential environmental and human health impacts of rechargeable lithium batteries in electronic waste

Environ. Sci. Tech., 47 (2013), pp. 5495-5503

M. Khan, I.M. Lo

A holistic review of hydrogel applications in the adsorptive removal of aqueous pollutants: recent progress, challenges, and perspectives

Water Res., 106 (2016), pp. 259-271

M. Kumar, B.P. Tripathi, V.K. Shahi

Crosslinked chitosan/polyvinyl alcohol blend beads for removal and recovery of Cd(II) from wastewater

J. Hazard. Mater., 172 (2–3) (2009), pp. 1041-1048

G.Z. Kyzas, D.N. Bikiaris

Recent modifications of chitosan for adsorption applications: a critical and systematic review

Mar. Drugs, 13 (2015), pp. 312-337

R. Laus, T.G. Costa, B. Szpoganicz, V.T. Fávere

Adsorption and desorption of Cu(II), Cd(II) and Pb(II) ions using chitosan crosslinked with epichlorohydrin-triphosphate as the adsorbent

J. Hazard. Mater., 183 (2010), pp. 233-241

J. Lemaire, L. Svecova, F. Lagallarde, R. Laucournet, P. Thivel

Lithium recovery from aqueous solution by sorption/desorption

Hydrometallurgy, 143 (2014), pp. 1-11

Q. Liang, E. Zhang, G. Yan, Y. Yang, W. Liu, X. Liu

A Lithium Ion-. -Impr. adsorbent Using Magn. Carbon nanospheres A Support Sel. Recovery Lithium ions. *N. Carbon Mater.*, 35 (6) (2020), pp. 696-706

J. Lie, S. Tanda, J.C. Liu

Subcritical water extraction of valuable metals from spent lithium-ion batteries

Molecules, 25 (9) (2020), p. 2166

C. Liu, B. Tao, Z. Wang, D. Wang, R. Guo, L. Liang Chen

Preparation and characterization of lithium ion sieves embedded in a hydroxyethyl cellulose cryogel for the continuous recovery of lithium from brine and seawater

Chem. Eng. Sci., 229 (2021), Article 115984

W. Liu, G. Yan, E. Zhang, Q. Liang, L. Qin, M. Wang, X. Liu, Yang Y

Extr. Lithium ions acidic Solut. Using Electrochem. Impr. Membr. Desalin., 496 (2020), Article 114751

Y. Ma, X. Zhou, J. Tang, X. Liu, H. Gan, J. Yang

One-step selective recovery and cyclic utilization of valuable metals from spent lithium-ion batteries via low-temperature chlorination pyrolysis

Resour. Conserv. Recy., 175 (2021), Article 105840

J. Mao, S. Lin, X.J. Lu, X.H. Wu, T. Zhou, Yeoung-Sang, Y.S. Yun

Ion-imprinted chitosan fiber for recovery of Pd(II): obtaining high selectivity through selective adsorption and two-step desorption

Environ. Res., 182 (2020), Article 108995

A. Masmoudi, G. Zante, D. Trébouet, R. Barillon, M. Boltoeva

Solvent extraction of lithium ions using benzoyltrifluoroacetone in new solvents

Separ. Purif. Technol., 255 (2021), Article 117653

P. Meshram, B.D. Pandey, T.R. Mankhand

Recovery of valuable metals from cathodic active material of spent lithium -ion batteries: leaching and kinetic aspects

Waste Manag., 45 (2015), pp. 306-313

M. Minceva, R. Fajgar, L. Markovska, V. Meshko

Comparative Study of Zn(II), Cd(II) and Pb(II) removal from water solution using natural clinoptilolitic zeolite and commercial granulated activated carbon. Equilibrium of adsorption

Sep. Sci. Technol., 43 (8) (2008), pp. 2117-2143

M. Monier, D.A. Abdel-Latif

Fabrication of Au(III) ion-imprinted polymer based on thiol-modified chitosan

Int. J. Biol. Macromol. 105 (2017), pp. 777-787

M. Monier, N.H. Elsayed, D.A. Abdel-Latif

Synthesis and application of ion-imprinted resin based on modified melamine-thiourea for selective removal of Hg(II)

Polym. Int., 64 (2015), pp. 1465-1474

M. Monier, D.A. Abdel-Latif, Y.G. Abou El-Reash

Ion-imprinted modified chitosan resin for selective removal of Pd(II) ions

J. Colloid Interface Sci., 469 (2016), pp. 344-354

M. Monier, A.L. Shafik, D.A. Abdel-Latif

Synthesis of azo-functionalized ion-imprinted polymeric resin for selective extraction of nickel (II) ions

Polym. Int., 67 (2018), pp. 1035-1045

M. Monier, A.A.H. Bukhari, N.H. Elsayed

Designing and characterization of copper (II) ion-imprinted adsorbent based on isatin functionalized chitosan

Int. J. Biol. Macromol., 155 (2020), pp. 795-804

M. Monier, I. Youssef, A. El-Mekabaty

Preparation of functionalized ion-imprinted phenolic polymer for efficient removal of copper ions

Polym. Int., 69 (2020), pp. 31-40

T. Naseri, N. Bahaloo-Horeh, S.M. Mousavi

Bacterial leaching as a green approach for typical metals recovery from end-of-life coin cells batteries

J. Clean. Prod., 220 (2019), pp. 483-492

P.A. Nashad, A. Bhaskarapillai, S. Velmurugan, S.V. Narasimhan

Cobalt (II) imprinted chitosan for selective removal of cobalt during nuclear reactor decontamination

Carbo. Poly., 87 (4) (2012), pp. 2690-2696

S. Natarajan, H.C. Bajaj, V. Aravindan

Template-free synthesis of carbon hollow spheres and reduced graphene oxide from spent lithium-ion batteries towards efficient gas storage

J. Mater. Chem. A., 7 (7) (2019), pp. 3244-3252

Nisola, G.M, Limjuco, L.A, Lawagon Vivas, E.L, M.J. C.P., Park, W.-J. Shon, H.K, W.J. Chung

Macroporous flexible polyvinyl alcohol lithium adsorbent foam composite prepared via surfactant blending and cryo-desiccation

Chem. Eng. J., 280 (2015), pp. 536-548

H.J. Park, N. Singhal, E.H. Jho

Lithium sorption properties of HMnO in seawater and wastewater

Water Res., 87 (2015), pp. 320-327

S.H. Park, K. Kim, J.H. Lim, S.J. Lee

Selective lithium and magnesium adsorption by phosphonate metal-organic framework-incorporated alginate hydrogel inspired from lithium adsorption characteristics of brown algae

Sep. Purif. Technol., 212 (2019), pp. 611-618

S.V. Pawar, G.D. Yadav

PVA/chitosan–glutaraldehyde cross-linked nitrile hydratase as reusable biocatalyst for conversion of nitriles to amides

J. Mol. Catal. B Enzym., 101 (2014), pp. 115-121

D. Permana, L.O. Ahmad, W. Ramadhan

Enhanced conductivity and ion exchange capacity of chitosan membranes through modification with lithium for lithium polymer battery application

WSEAS Trans. Power Syst., 11 (2017), pp. 183-189

L. Pozzo, Y. de, T.F. Conceição, A. da., Spinelli, N. Scharnagl, A.T.N. Pires

The influence of the crosslinking degree on the corrosion protection properties of chitosan coatings in simulated body fluid

Prog. Org. Coatings, 137 (2019), Article 105328

W. Qi, J.G. Shapter, Q. Wu, T. Yin, G. Gao, D.X. Cui

Nanostructured anode materials for lithium-ion batteries: principle, recent progress and future perspectives

J. Mater. Chem. A., 5 (2017), pp. 9521-9540

C. Qin, H. Li, Q. Xiao, Y. Liu, J. Zhu, Y. Du

Water-solubility of chitosan and its antimicrobial activity

Carbohydr. Polym., 63 (2006), pp. 367-374

Y. Qin, X. Chen, B. Li, Y. Guo, Z. Niu, T. Xia, W. Meng, M. Zhou

Study on the mechanical properties and microstructure of chitosan reinforced metakaolin-based geopolymer

Constr. Build. Mater., 271 (2021), Article 121522

T. Ryu, Y. Haldorai, A. Rengaraj, J. Shin, H.J. Hong, G.W. Lee, K.S. Chung

Recovery of lithium ions from seawater using a continuous flow adsorption column packed with granulated chitosan-lithium manganese oxide

Ind. Eng. Chem. Res., 55 (26) (2016), pp. 7218-7225

T. Ryu, A. Rengaraj, Y. Haldorai, J. Shin, S.R. Choe, G.W. Lee, K.S. Chung

Mechanochemical synthesis of silica-lithium manganese oxide composite for the efficient recovery of lithium ions from seawater

Solid State Ion., 308 (2017), pp. 77-83

M. Sethurajan, S. Gaydardzhiev

Bioprocessing of spent lithium ion batteries for critical metals recovery – a review

Resour. Conserv. Recy., 165 (2021), Article 105225

B. Swain

Recovery and recycling of lithium: a review

Separ. Purif. Technol., 172 (2017), pp. 388-403

A.A. Taha, M.A. Shreadah, A.M. Ahmed, H.F. Heiba

Multi-component adsorption of Pb(II), Cd(II), and Ni(II) onto Egyptian Na-activated bentonite; equilibrium, kinetics, thermodynamics, and application for seawater desalination

J. Environ. Chem. Eng., 4 (2016), pp. 1166-1180

S. Tang, J. Yang, L. Lin, K. Peng, Y. Chen, S. Jin, W. Yao

Construction of physically crosslinked chitosan/sodium alginate/calcium ion double-network hydrogel and its application to heavy metal ions removal

Chem. Eng. J., 393 (2020), Article 124728

M. Vanitha, N. Balasubramanian

Waste minimization and recovery of valuable metals from spent lithium-ion batteries—a review

H. Vikstrom, S. Davidsson, M. Hook

Lithium availability and future production outlooks

Appl. Energy, 110 (2013), pp. 252-266

R. Vimala, D. Charumathi, N. Das

Packed bed column studies on Cd(II) removal from industrial wastewater by macrofungus *Pleurotus platypus*

Desalination, 275 (1–3) (2011), pp. 291-296

S.A. Wahib, D.A. Da'na, N. Zaouri, Y.M. Hijji, M.A. Al-Ghouti

Adsorption and recovery of lithium ions from groundwater using date pits impregnated with cellulose nanocrystals and ionic liquid

J. Hazard. Mater., 421 (2022), Article 126657

B. Wang, F. Liu, F. Zhang, M. Tan, H. Jiang, Y. Liu, Y. Zhang

Efficient separation and recovery of cobalt(II) and lithium(I) from spent lithium ion batteries (LIBs) by polymer inclusion membrane electro dialysis (PIMED)

Chem. Eng. J., 430 (2022), Article 132924

M. Wang, C. Zhang, F. Zhang

An environmental benign process for cobalt and lithium recovery from spent lithium-ion batteries by mechanochemical approach

Waste Manag., 51 (2016), pp. 239-244

W. Wang, Y. Wu

An overview of recycling and treatment of spent LiFePO₄ batteries in China

Resour. Conserv. Recycl., 127 (2017), pp. 233-243

S. Wei, Y. Wei, T. Tao Chen, C. Liu, Y. Tang

Porous lithium ion sieves nanofibers: general synthesis strategy and highly selective recovery of lithium from brine water

Chem. Eng. J., 379 (2020), Article 122407

W. Wu, X. Liu, X. Zhang, X. Li, Y., Zhu, M. Qiu, W. Tan

Mechanism underlying the bioleaching process of LiCoO₂ by sulfur-oxidizing and iron-oxidizing bacteria

J. Biosci. Bioeng., 128 (3) (2019), pp. 344-354

J. Xiao, B. Niu, Z. Xu

Highly efficient selective recovery of lithium from spent lithium-ion batteries by thermal reduction with cheap ammonia reagent

J. Hazard. Mater., 418 (2021), Article 126319

E. Yang, K.J. Chae, M.J. Choi, Z. He, I.S. Kim

Critical review of bioelectrochemical systems integrated with membrane-based technologies for desalination, energy self-sufficiency, and high-efficiency water and wastewater treatment

Desalination, 452 (2019), pp. 40-67

K. Yoshizuka, K. Fukui, A. Inouek

Selective recovery of lithium from seawater using a novel MnO₂ type adsorbent

Ars. Sep. Acta, 1 (2002), pp. 79-86

A. Youngwilai, P. Kidkhunthod, N. Jearanaikoon, J. Chaiprapa, N. Supanchaiyamat, A.J. Hunt, Y. Ngernyen, T. Ratpukdi, E. Khan, S. Siripattanakul-Ratpukdi

Simultaneous manganese adsorption and biotransformation by *Streptomyces violarius* strain SBP1 cell-immobilized biochar

Sci. Total Environ., 713 (2020), Article 136708

H. Yu, P. Shao, L. Fang, J. Pei, L. Ding, Pavlostathis

Palladium ion-imprinted polymers with PHEMA polymer brushes: role of grafting polymerization degree in anti-interference

Chem. Eng. J., 359 (2019), pp. 176-185

X. Zeng, J. Li, N. Singh

Recycling of spent lithium-ion battery: a critical review

Crit. Rev. Environ. Sci. Tech., 44 (10) (2014), pp. 1129-1165

J. Zhang, J. Hu, W. Zhang, Y. Chen, C. Wang

Efficient and economical recovery of lithium, cobalt, nickel, manganese from cathode scrap of spent lithium-ion batteries

J. Clean. Prod., 204 (2018), pp. 437-446

L. Zhang, L. Li, H. Rui, D. Shi, X. Peng, L. Ji, X. Song

Lithium recovery from effluent of spent lithium battery recycling process using solvent extraction

J. Hazard. Mater., 398 (2020), Article 122840

Q.H. Zhang, S.P. Li, S.Y. Sun, X.S. Yin, J.G. Yu

LiMn₂O₄ spinel direct synthesis and lithium ion selective adsorption

Chem. Eng. Sci., 65 (1) (2010), pp. 169-173

T. Zheng, J. Li, Y. Ji, W. Zhang, Y. Fang, F. Xin, W. Dong, P. Wei, J. Ma, M. Jiang